DEUTSCHES ELEKTRONEN-SYNCHROTRON **DESY**

DESY 86-096
August 1986

CAUSTICS IN A SIMPLE SU(2) LATTICE GAUGE THEORY MODEL

by

J. Bartels

II. Institut f. Theor. Physik, Universität Hamburg

T.T. Wu

Deutsches Elektronen-Synchrotron DESY, Hamburg

and

Gordon McKay Lab., Harvard University, Cambridge

ISSN 0418-9833

NOTKESTRASSE 85 · 2 HAMBURG 52

To be sure that your preprints are promptly included in the
HIGH ENERGY PHYSICS INDEX ,
send them to the following address (if possible by air mail) :

DESY
Bibliothek
Notkestrasse 85
2 Hamburg 52
Germany

DESY 86-096
August 1986

ISSN 0418-9833

Caustics in a Simple SU(2) Lattice Gauge Theory Model

J. Bartels
II. Institut für Theoretische Physik, Universität Hamburg

Tai Tsun Wu *
Deutsches Elektronen-Synchrotron, Hamburg
and
Gordon McKay Laboratory, Harvard University, Cambridge, Mass.

Abstract

This paper describes the beginning of an attempt to study the weak coupling limit of lattice gauge theories, using the Hamiltonian formulation and the semiclassical approximation. The topics are caustics and the behavior of the ground state wave function in the vicinity of caustics. For two very simple SU(2) models (one plaquette, two plaquettes) we demonstrate the existence of caustics, determine their locations and study the peaking behavior of the ground state wave function on them in the limit $g^2 \to 0$.

* Work supported in part by the US Department of Energy under Grant DE-FG 02-84ER40158

I. Introduction

Lattice gauge theories [1] on a finite volume have been studied quite intensely during the past years [2]. For the limit of large lattice coupling constant the strong coupling expansion [3] has been used to prove confinement and to calculate various physical quantities of interest. Existing calculations [4] extend over large orders of the inverse coupling constant. For smaller values of the coupling constant where this expansion can no longer be used computer simulations [5] (Monte Carlo calculations) have been performed [2]. In both the strong and the weak coupling regimes they are consistent with the expected behavior: for large coupling constants they match the results for the strong coupling expansion, whereas in the weak coupling region they do not contradict the scaling behavior predicted by the renormalization group equation [6]. For example, for a physical mass the expected behavior is:

$$m_{phys} = const \cdot \frac{1}{a} \cdot \exp\left[-\frac{1}{2\beta_0 g^2}\right] \cdot (\beta_0 g^2)^{-\beta_1/2\beta_0^2} \cdot [1 + O(g^2)] \qquad (1.1)$$

(β_0, β_1, are the coefficients of the β-function, a is the lattice distance, and the constant is the quantity to be read off from the numerical computer analysis). The status of analytic calculations in the weak coupling regime is much less satisfactory than that in the strong coupling region. For U(1) gauge theory in 3 dimensions Göpfert and Mack [7] have shown that confinement holds for all values of the coupling constant, but for nonabelian theories an analogous proof is not available. Note that for these theories it is the weak coupling regime which is relevant for the continuum limit.

A natural framework for analytic investigations of lattice gauge theorie is the Hamiltonian formulation [8]. Based on the Hamiltonian of Kogut and Susskind [8] several attempts have been made for solving the Schrödinger equation, in particular

for the ground state wave function. Motivated by a successful variational calculation in compact Quantum Electrodynamics in 2+1 dimensions [9], various variational techniques have been explored [10] first in the abelian U(1)-case in 2+1 and 3+1 dimensions, then also in the nonabelian SU(2) [11] and SU(3) [12] cases. Other calculations make use of the t-expansion [13] or Lanczos' method [14]. None of these authors claim to have a systematic study of the extreme weak coupling limit. The behaviour in the limit of small coupling constant, however, is used as an important test for the quality of the approximation.

Systematic perturbative studies of the weak coupling limit in the Hamiltonian formulation have been started by Lüscher [15] and Müller and Rühl [16]. The latter deals with SU(2)-lattice gauge theory in 2+1 dimensions and calculates, to leading order in powers of the coupling constant, the energy gap and the static potential. The first approach (calculations are done in the continuum limit directly) makes use of the fact that for small spatial volume the effective coupling constant is small: the size of the volume therefore controls the validity of the perturbation expansion, and one expects that perturbation theory gives a reliable answer for small-size models. With increasing volume, of course, corrections due to tunneling effects have to be included [17].

The standard method for studying tunneling effects in quantum mechanical systems is the semiclassical approximation. The particular g^2-dependence of the lattice Hamiltonian [8]:

$$H = \frac{g^2}{2} T + \frac{2}{g^2} V \qquad (1.2)$$

(T is the electric part and plays the rôle of the kinetic energy, V represents the magnetic part and provides the potential) suggests to attack the $g^2 \to 0$ limit of (1.2) by the same method as one treats the limit $\hbar \to 0$ in ordinary

quantum mechanics (i.e. g^2 plays the rôle of $\hbar$). This then leads to Hamiltonian classical mechanics in a system of many degrees of freedom. Several years ago instanton contributions [18] to the (euclidean) partition function of gauge theories have been investigated quite extensively; since the integration over the size of the instanton configurations diverges, it has remained unclear whether instanton configurations in the functional integral could be a useful starting point. In principle one expects that analogous configurations exist also on the lattice and show up in the limit $g^2 \to 0$; if these contributions were the only effect seen in a semiclassical approximation to (1.2), an analysis of this type would not appear to be very promising. It is, however, well-known that a semiclassical analysis of a quantum mechanical problem has many more facets [19] [20], such as foci, caustics, shadow, Young's phenomenon; it is also very likely that phenomena of modern nonlinear mechanics [21] such as chaotic behavior play a rôle. We therefore feel that the idea of applying the full apparatus of the semiclassical approximation to the weak coupling limit of (1.2) looks sufficiently promising, and an attempt should be made.

In this paper we describe an exploratory study of a simple SU(2) lattice model (without fermions) which exhibits some of those features which we expect to be relevant for a larger realistic lattice model. In order to analyse the ground state of (1.2) in the semiclassical approximation, one solves the corresponding classical equations of motion: the solutions start in the region of small fields, where the ground state wave function is of order unity, and then spread out in configuration space, where the wave function decreases exponentially. It is therefore natural to study first classical solutions at distances not too far away from the point of zero fields. At very large distances the exponential suppression makes it less probable that the details of the ground state wave function matter. At finite distances the most prominent feature of the classical solutions are

caustics, i.e. regions in configuration space where neighboring trajectories intersect. It is this phenomenon on which we concentrate in this paper.

In order to investigate the influence of caustics on the ground state wave function in some detail we have chosen to study the simplest nonabelian lattice models: one consisting of one single plaquette, the other of two plaquettes. In both cases we use free boundary conditions *): the classically allowed region then consists of one isolated point, the origin. The classical solutions we are interested in have energy zero and leave the origin in all possible directions of configuration space. Although focal points and caustics in the semiclassical approximation to quantum mechanics have been known for a long time, it is only more recently [20] that a formulation has been given which allows generalization to higher numbers of variables. In this formulation, caustics are related to singularities of mappings, and Arnold [22] has given a complete list of normal forms of stable singularities for the Hamilton-Jacobi function S for spatial dimensions ≤ 5. This classification has turned out to be very useful for us, although our models also contain singularities which are not on this list (they correspond to unstable singularities). The most striking feature of the ground state wave function is that on the caustic it develops a peak in the limit $g^2 \to 0$:

$$\psi \sim \text{const.}\ g^{-p} \exp\left[-1/g^2\, S(\bar{A})\right]. \qquad (1.3)$$

Here p is a positive fractional power which depends upon the detailed structure of the caustic; $\bar{A}$ denotes the coordinates of the point on the caustics, and the normalization of the wave function is such that for a regular point (not on the caustic) the-factor in front of the exponential is independent of g^2. Our main effort has been to establish for our models the appearance of caustics in the case of SU(2) gauge theory and then to find, in the vicinity of the most interesting parts of the caustic, the form (1.3) for the wave function.

This paper will be organized as follows. We first (Section II) present a brief summary of the semiclassical approximation. In particular we say a few words about the classification of caustics as stable singularities of mappings. As a first illustration we then (Section III) apply the semiclassical approximation to the simplest model, consisting of one single plaquette. Because of the high symmetry, this model does not yet fully exhibit the phenomenon which we want to explore. We therefore in Section IV turn to the next simplest model which consists of two plaquettes. Here we first use the computer for locating the caustics, then we construct the ground state wave function in the vicinity of the most interesting parts of the caustic. In the last section we summarize and give a brief discussion. Some details of analytic calculations are put into two appendices.

*) For the case of periodic boundary conditions Lüscher [15] has shown that the potential has valleys (toron configurations). It is for this complication that we have chosen to use, for the beginning, free boundary conditions.

II. Semiclassical Method in Quantum Mechanics

The generic form of the Schrödinger equation which is to be solved in the limit $\hbar \to 0$ is the following *):

$$\left[-\frac{\hbar^2}{2} G^{ab}(x) \left(\frac{\partial^2}{\partial x^a \partial x^b} - \Gamma^c_{ab} \frac{\partial}{\partial x^c} \right) + V(x) \right] \psi(x) = E \psi(x) \ . \tag{2.1}$$

Here a, b = 1, ..., N; $G^{ab}(x)$ is the real, symmetric, and positive definite metric tensor, and Γ^c_{ab} are the connection coefficients:

$$\Gamma^c_{ab} = \frac{1}{2} G^{cm} \left(\frac{\partial G_{mb}}{\partial x^a} + \frac{\partial G_{ma}}{\partial x^b} - \frac{\partial G_{ab}}{\partial x^m} \right). \tag{2.2}$$

There are two equivalent ways of deriving the semiclassical approximation. The first one is usually presented in textbooks on quantum mechanics (see, e.g., Ref. 23). With the ansatz

$$\psi(x) = A(x) \cdot \exp \left[\frac{i}{\hbar} \tilde{S}(x) \right] \tag{2.3}$$

$$\tilde{S}(x) = S(x) + O(\hbar^2) \tag{2.4}$$

one goes into the Schrödinger equation (2.1) and derives differential equations for the functions S (x) and A(x):

$$G^{ab}(x) \frac{\partial S}{\partial x^a} \cdot \frac{\partial S}{\partial x^b} = 2 \left[E - V(x) \right] \tag{2.5}$$

or $$S^{;a} S_{;a} = 2 \left[E - V(x) \right] ,$$

*) This $\hbar$ is merely a small parameter and will be identified later with $-ig^2$.

$$G^{ab}(x) \left(A^2 \frac{\partial S}{\partial x^b} \right)_{;a} = 0$$

or $$\left(A^2 S^{;a} \right)_{;a} = 0 \ , \tag{2.6}$$

where $;a$ is the covariant derivative:

$$\left(A^2 \frac{\partial S}{\partial x^b} \right)_{;a} = \frac{\partial}{\partial x^a} \left(A^2 \frac{\partial S}{\partial x^b} \right) - \Gamma^c_{ab} \left(A^2 \frac{\partial S}{\partial x^c} \right) . \tag{2.7}$$

Both equations (2.5) and (2.6) can be solved if we know the solutions of the classical equations of motion of the Hamiltonian

$$H(p,x) = \frac{1}{2} G^{ab}(x) p_a p_b + V(x) \ . \tag{2.8}$$

Since eq. (2.5) is the same as

$$H \left(\frac{\partial S}{\partial x}, x \right) = E \ , \tag{2.5'}$$

the solution is given by the action integral

$$S(x) = \int_{x_0}^{x} p_a \, dq^a \ . \tag{2.9}$$

The line integral goes along the classical trajectory which connects the points x_0 and x and has energy E. The point x_0 is specified through the boundary condition which $\psi(x)$ has to obey. Similarly, the continuity equation (2.6) is solved by:

$$A^2(x) = \text{const.} \exp \left[- \int_{x_0}^{x} d\sigma \, \frac{G^{ab} \left(\frac{\partial S}{\partial x^b} \right)_{;a}}{\sqrt{G^{ab} \frac{\partial S}{\partial x^a} \frac{\partial S}{\partial x^b}}} \right] , \tag{2.10}$$

where $d\sigma = \sqrt{G_{ab} dx^a dx^b}$ is the differential of the arclength, and the line integral again goes along the classical trajectory.

Equivalently, one could start from Feynman's path integral [24] representation of the time-independent Schrödinger wave function

$$\psi(x) = \int [dx] \exp\left[\tfrac{i}{\hbar} \int_{x_0}^{x} p_a \, dq^a \right] , \tag{2.11}$$

Here the integration goes over all paths which connect the points x_0 and x and have energy E; $p_a = \frac{\partial \mathcal{L}}{\partial \dot{x}^a}$, and $\mathcal{L} = \frac{1}{2} G_{ab} \dot{x}^a \dot{x}^b - V$. In the limit $\hbar \to 0$ the classical path dominates and

$$\psi(x) \approx A(x) \exp\left[\tfrac{i}{\hbar} \int_{x_0}^{x} p_a \, dq^a \right]. \tag{2.12}$$

This is the same as (2.9), but the prefactor A now represents the quantum fluctuations around the classical path between x_0 and x. Under normal circumstances the leading contribution to A (in the limit $\hbar \to 0$) comes from the gaussian fluctuations, but as we will discuss later, it may happen that one has to keep more than quadratic terms in the exponent of (2.11).

In a given problem it may happen that the wave function $\psi(x)$ is known already in some region of configuration space. Then the task will be to find $\psi(x)$ in the remaining part of configuration space by means of the semiclassical approximation. To be specific, let $\psi(x)$ be known in a bounded region D with boundary Σ_0. We then know the functions S (x) and A(x) on Σ_0 and can use this information to set up the classical problem: for any $x_0 \in \Sigma_0$ we have $p_a = \frac{\partial S}{\partial x^a}\Big|_{x_0}$ which uniquely fixes the classical trajectory through x_0. Now let us assume that for any x outside of D and not too far away from Σ_0 there is exactly one trajectory which connects x

with some point $x_0 \in \Sigma_0$. We then have a unique prescription for calculating (2.9) and also (2.10) and, hence, for calculating the wave function $\psi(x)$ at the point x. This will remain true also further away from Σ_0, until we reach a point where different trajectories coming from Σ_0 intersect.

Before we start to discuss this phenomenon in more detail let us describe how the semiclassical approximation works in a lattice gauge theory calculation. The Hamiltonian has the form [8]:

$$H = \frac{g^2}{2} T + \frac{2}{g^2} V , \tag{2.13}$$

where the electric part T consists of a second order differential operator with a positive definite metric (in its form it agrees with the differential operator of eq. (2.11)), and the magnetic part V is a positive semidefinite function of the group elements associated with the links of the lattice. In order to compare with eq. (2.1) we note that the ground state energy of (2.13) goes as O(1) when $g^2 \to 0$. After multiplication with g^2 the Schrödinger equation takes the form

$$\left[\frac{g^4}{2} T + 2V \right] \psi = g^2 E \psi , \tag{2.14}$$

which explicitly shows the dependence upon g^2. For small g^2, the classically allowed region shrinks to those points where the potential V vanishes. If we choose free boundary conditions, V = 0 only for zero fields; for periodic boundary conditions the potential vanishes on a manifold of dimension > 0 [25] (a more detailed discussion is given in Ref. 15). There exist other types of boundary conditions for which V vanishes on a set of isolated points: an example for this is presented in Appendix A. In the main part of this paper we will work only with free boundary conditions. This is the simplest case, since the classically allowed region is just the one point where all field variables vanish.

Now since in the classically allowed region both V and g^2E are zero, we know from eq. (2.5) that $\frac{\partial S}{\partial x^a} = 0$. Therefore S = const on each connected component of the classically allowed region, and also $p_a = \frac{\partial S}{\partial x^a} = 0$. This then determines the starting condition of the classical trajectories: for the case of free boundary conditions we search for classical trajectories of zero energy which start at the origin with momentum zero. For a complete calculation of the semiclassical wave function, however, we need more than the starting values of the classical solution: we also have to know the starting value of the prefactor A (i.e. the constant in (2.10)). This information is easily obtained from the quadratic approximation to (2.14) and its solution, the gaussian wave function. If we would work with periodic boundary condition, this last question would be significantly more difficult: the solution can be found in Ref. 15.

We now return to intersection points of classical trajectories. This phenomenon is most conveniently phrased in terms of geodesics and curvature. It is well known [20] that a classical trajectory which connects two points x_o and x_1 minimizes the action integral

$$S = \int_{x_o}^{x} p_a \, dq^a \,. \tag{2.15}$$

Here the variation goes over all paths from x_o to x_1, which have constant energy $E = H(p,q)$. Using the equations of motion

$$\dot{q}^a = \frac{\partial H}{\partial p_a} = G^{ab} p_b \tag{2.16}$$

and the relation between time and arclength

$$d\sigma = \sqrt{G_{ab}\, \dot{q}^a \dot{q}^b}\; dt = \sqrt{2\,[E-V]}\; dt, \tag{2.17}$$

eq. (2.13) can also be written as

$$S = \int_{x_o}^{x_1} \sqrt{2\,[E-V]}\; d\sigma. \tag{2.18}$$

Trajectories which minimize this integral can, formally, be viewed as geodesics in a space with a metric

$$\tilde{G}^{ab} = 2\,[E-V]\, G^{ab}. \tag{2.19}$$

Let $\tilde{R}^a_{bcd}$ be the corresponding Riemann curvature tensor, and let us consider a continous set of geodesics $x^a(\sigma,\alpha)$ through the point x_o (σ denotes the arclength, α labels the geodesics). Then the vector $\frac{dx^a}{d\sigma}(\sigma,\alpha)$ is tangential to the geodesic $x^a(\sigma,\alpha)$, whereas the vector $v^a = \frac{dx^a}{d\alpha}(\sigma,\alpha)\big|_{\alpha=0}$ measures the deviation of an infinitesimally neighboring geodesic from the geodesic $x^a(\sigma,0)$. Obviously, $v^a = 0$ if the two geodesics intersect. Such a point is called conjugate to x_o or focal point. The vector v^a satisfies the equation for geodesic deviation (Jacobi equation)[26]

$$\frac{D^2}{d\sigma^2} v^a + \tilde{R}^a_{bcd}\, \frac{dx^b}{d\sigma}\, \frac{dx^c}{d\sigma}\, v^d = 0 \,. \tag{2.20}$$

Here $\frac{D}{d\sigma}$ denotes the covariant derivative along the geodesic:

$$\frac{Dv^a}{d\sigma} = v^a_{\;;b}\, \frac{dx^b}{d\sigma} \,. \tag{2.21}$$

Equation (2.20) has an obvious interpretation: the curvature tensor $\tilde{R}$ acts like a force on the vector v. Depending on the sign and size it either pushes neighboring geodesics apart or causes them to intersect. In particular, if $\tilde{R}$ is zero the geodesics do not intersect. This shown quite clearly that it is the presence of curvature which is responsible for focal points.

If on a geodesic $x^a(\sigma, \alpha = 0)$ a focal point exists, it will, in general also exist on other geodesics nearby. The locus of these focal points is called caustic . In N-dimensional configuration space the caustic forms a manifold Σ_f of dimension less than N. The shape of Σ_f can be rather complicated, but useful information can be obtained from Arnold's list of generic singularities [20), 22)].

The basic idea is to relate the caustic to stable singularities of smooth mappings for which mathematical literature is available. In the 2N-dimensional (pq)-space each function S(q,t) describes, by virtue of $p_a = \frac{\partial S}{\partial q^a}$, a N-dimensional surface whose shape changes as a function of time. For simplicity consider the case N = 1 (Fig. 1). At some time t_o S may have the form shown in Fig. 1a: for each q there is one value $p = \frac{\partial S}{\partial q}$. At some later time $t > t_o$ S has a different shape, as shown in Fig. 1b. For some values of q there are two values $p = \frac{\partial S}{\partial q}$, for other q's there are none. In terms of classical trajectories, for $t = t_o$ one classical trajectory passes through each point, whereas for $t > t_o$ some points are reached by two different trajectories, others by none. It is convenient to introduce, for each S(q,t), the map $\pi: p \to q$. It is the inverse of the equation $p = \frac{\partial S}{\partial q}$. With the Legendre-transform $f = pq - S$ we have $q = \frac{\partial f}{\partial p}$. In Fig. 1a the map π is smooth, whereas in Fig. 1b there is a singularity marked by the dashed line. To the right there are two preimages of this map, on the left hand side there is no preimage. The general task is then to classify singularities of mappings π:

$p \to q$; because of $q^a = \frac{\partial f}{\partial p_a}$ we are particularly interested in derivative maps. In Refs. 20, 22 Arnold presents a list of normal forms in the neighborhood of these singularities. With a little algebra it is possible to deduce from them the shape of the caustic Σ_f. In the following sections we shall discuss examples which arise in our model calculations: in some of the cases we can make immediate use of Arnold's list of singularities. There are, however, also singularities which are not contained in this list: these are unstable singularities.

We now return to our wave function $\psi(x)$ which we have started to construct by means of the semiclassical approximation. As long as each point x is reached by one classical trajectory, $\psi(x)$ is represented by a single term (2.12), as we have outlined above. Beyond a focal point, however, points x may be reached by more than one trajectory. The wave function $\psi(x)$ then consists of several terms of the form (2.12):

$$\psi(x) = \sum_j A_j(x) \exp\left[\tfrac{i}{\hbar} \int_{x_{oj}}^{x} p_a \, dq^a + \tfrac{i\pi}{2} \mu_j \right]. \qquad (2.22)$$

Here, for a given x, the sum over j runs over all classical trajectories which connect the point x with some point x_{oj} on the initial surface x_o. For each such trajectory the index μ_j counts the number of focal points between x_{oj} and x (Morse index). As we have said before, in lattice gauge theories with free boundary conditions all trajectories start at the origin, so $x_{oj} = 0$. It is clear from (2.22) that a focal point represents a singularity of the semiclassical approximation to $\psi(x)$. Before the focal point $\psi(x)$ consists of one piece, after it $\psi(x)$ has the form (2.22). What becomes singular is the prefactor A(x). This is most easily seen if we use Riemann normal coordinates [26)] y^a rather than the previous system x^a. Consider again the classical trajectories as geodesics in a curved space (2.19), starting from x_o. In addition to our reference trajectory

$x^a(\sigma)$, take N-1 linearly independent and infinitesimally neighboring geodesics $x_i^a(\sigma)$ (i = 1, ..., N-1). They could be labelled, for instance, by a set of N-1 angles relative to the reference trajectory $x^a(\sigma)$, by which they leave the point x_o. At the focal point, some linear combination of them will intersect with $x^a(\sigma)$. The new coordinates y^a are the arclength σ and these N-1 angles. Because of (2.9) and (2.18), the arclength is the same as S . Along each of these trajectories, the y^2, ..., y^N stay constant. The metric tensor G_{ab} transforms into:

$$\tilde{G}_{ab} \to \tilde{G}_{a'b'} \frac{dx^{a'}}{dy^a} \cdot \frac{dx^{b'}}{dy^b}$$

$$\det \tilde{G} \longrightarrow \det \tilde{G} \cdot \left| \frac{dx}{dy} \right|^2 = \overline{G} . \qquad (2.23)$$

The covariant derivative of S simply becomes:

$$S_{;a} = \frac{\partial S}{\partial y^a} = \delta_{a1}$$

$$S^{;a} = \tilde{G}^{aa'} S_{;a'} = \tilde{G}^{a1} = \delta^{a1} \tilde{G}^{11} . \qquad (2.24)$$

In the last line we have used the fact that in Riemann normal coordinates $\tilde{G}^{a1} \sim \delta^{a1}$ and $\tilde{G}^{1a} \sim \delta^{1a}$. Eq. (2.6) in these coordinates simplifies:

$$0 = \left(A^2 S^{;b}\right)_{;b} = \frac{1}{\sqrt{\tilde{G}}} \frac{\partial \left(\sqrt{\tilde{G}}\, A^2 S^{;b}\right)}{\partial y^b}$$

$$= \frac{1}{\sqrt{\tilde{G}}} \frac{\partial \left(\sqrt{\tilde{G}}\, A^2 \tilde{G}^{11}\right)}{\partial y^1} . \qquad (2.25)$$

Along the trajectory $y^a(t)$:

$$const = \sqrt{\tilde{G}}\, A^2\, \tilde{G}^{11}$$

or

$$A^2 = \frac{const. \cdot \tilde{G}_{11}}{\sqrt{\tilde{G}}} . \qquad (2.26)$$

At the focal point the transformation $x \to y$ becomes singular, i.e. the Jacobian determinant $\left|\frac{\partial x}{\partial y}\right|$ vanishes. Hence $\overline{G} = \det \tilde{G} \cdot \left|\frac{dx}{dy}\right|^2$ becomes zero, and A is singular. The same can be seen in the path integral (2.11): at the focal point two minima of the action integral $\int p_a dq^a$ coincide. Therefore, one of the eigenvalues of the matrix of second variations must be zero, and the prefactor A in (2.12) from the gaussian fluctuations becomes singular.

The appearance of such a singularity near a focal point only signals that the semiclassical approximation breaks down. In principle, one has to solve the Schrödinger equation near the focal point more accurately than it is done in eqs. (2.5) and (2.6). In the examples that we will present below it is sufficient to approximate in (2.1) the metric and the potential by their constant values at the focal point. We then search for a superposition of plane waves which away from the focal point matches the behavior obtained from the semiclassical approximation. This procedure divides the configuration space into two parts: there is an inner region near the caustic where the "naive" semiclassical approximation (2.3) cannot be used. The size of this region scales with some fractional power of $\hbar$, and the power depends upon the detailed shape of Σ_f. In the outer region (2.3) or (2.22) are valid approximations. At fixed $\hbar$, $\psi(x)$ as a function of x is perfectly well-behaved. But if we let $\hbar \to 0$ for fixed x, then $\psi(x)$ is singular on a caustic: relative to a point away from the caustic, $A(x)$ scales with a negative, fractional power of $\hbar$:

$$\psi(x_{caustic}) = const \cdot \hbar^{-p} \exp\left[i/\hbar \, S(x_{caustic}) \right] . \qquad (2.27)$$

The value of the exponent p depends upon the detailed structure of Σ_f.

In the following we shall present the two simplest examples which illustrate all the features outlined above. In case of the two-plaquette problem (Section IV) we have found it convenient to proceed in the following way: a) first establish the existence of a caustic and the behavior of classical trajectories in the neighbourhood; b) use Arnold's list of normal forms to find (up to a smooth transformation of variables) the function S; c) from a local approximation to the Schrödinger equation at the focal point find the solution which, away from the caustic, matches the semiclassical approximation. This solution shows the singular behavior of the prefactor A near the caustic or, equivalently, the behavior (2.27) when $\hbar \to 0$. d) Finally, replace $i/\hbar \to -1/g^2$ which leads to the situation of lattice gauge theories.

III. The One-Plaquette Problem

As a first illustration of the ideas outlined in the previous section we consider a single plaquette with free boundary conditions. This simple quantum mechanical system has been investigated by several authors [27].

The notation is indicated in Fig. 2. For each link variable we use the parametrization $U_i = x_{i0} + i \vec{x}_i \vec{\sigma}$, $x_{i0}^2 + \vec{x}_i^2 = 1$ (i = 1, ..., 4), and the Hamiltonian takes the form

$$H = -\frac{g^2}{8} \sum_{i=1}^{4} \Delta_i' + \frac{2}{g^2} tr\left[1 - U_1 U_2 U_3^{-1} U_4^{-1} \right] . \qquad (3.1)$$

Here Δ stands for the Laplacian in 4 dimensions, and the prime indicates that the variables are restricted to the surface of the unit sphere. It is convenient to use 4 dimensional polar coordinates. The link variables then are $x_{i0} = \cos\theta_i$, $\vec{x}_i = \sin\theta_i (\sin\vartheta_i \cos\varphi_i, \sin\vartheta_i \sin\varphi_i, \cos\vartheta_i)$, and the Laplacian Δ' takes the form:

$$\Delta_i' = \frac{\partial^2}{\partial\theta_i^2} + 2 \operatorname{ctg}\theta_i \frac{\partial}{\partial\theta_i} + \frac{1}{\sin^2\theta_i} \vec{L}_i^2 , \qquad (3.2)$$

where $\vec{L}_i$ is the usual angular momentum vector operator expressed in term of polar coordinates.

We now have two options to continue. According to the strategy outlined above we would first solve the Schrödinger equation with (3.1) in the quadratic approximation. For the ground state this leads to a gaussian wave function, the exponent of which has the form $-1/g^2 \, S(x_1, x_2, x_3, x_4)$. It is manifestly gauge invariant. We then would use S for defining the starting conditions for the classical equations of motion. The solution to this again preserves gauge invariance,

such that the resulting expressions for S and A are also invariant under gauge transformations. The number of variables that we are dealing with is 4 x 3 = 12; from the gauge fixing procedure outlined in Ref. 28 we know that the number of independent variables is much smaller. By applying suitable gauge transformations to the variables U_1, ..., U_4 we can fix the SU(2) elements $U_1 = U_2 = U_4 = 1$. After this there is still invariance left under a global gauge transformation which leaves us with only one degree of freedom. Therefore, if we encounter a focal point along some trajectories in our 12-dimensional space it well, in fact, lie on a hypersurface of dimension ≤ 11. Displacements within this surface are generated by gauge transformations which correspond to a symmetry of our Hamiltonian.

For practical reasons it is therefore advantagous to eliminate all gauge degrees of freedom from the start (this does not hold for more complicated lattice models, e.g. already a 1^3-cube). Following the procedure of Bronzan [28], we fix the SU(2)-elements along the maximal gauge tree which consists of the links 4, 1, and 2. This leaves us with the Hamiltonian

$$H = -\frac{g^2}{8}\Delta' + \frac{4}{g^2}\left[1 - \cos\theta\right] , \tag{3.3}$$

where all angles now belong to the loop variables $U = U_1 U_2 U_3^{-1} U_4^{-1}$. There is still gauge freedom left: a global SU(2) rotation which for all variables U_1, U_2, U_3, U_4 and U means a "spatial" rotation of the angles ϑ and φ. The ground state wave function must be invariant under these rotations, i.e. it has "angular momentum" zero. By eliminating in this way the dependence upon ϑ and φ, eq. (3.3) reduces to an ordinary differential euquation: by a simple change of variables it is possible to solve this equation in terms of Mathieu-functions [27]. For various reasons, however, we wish to apply a semiclassical analysis.

First we solve eq. (3.3) in the quadratic approximation. Clearly the lowest energy, rotationally invariant, and normalizable solution is

$$\psi_0(\theta) = N \cdot \exp\left[-2/g^2 \cdot \theta^2\right] \tag{3.4}$$

with energy eigenvalue $E = 3/2$, and the function S can be read off as

$$S = 2\,\theta^2 . \tag{3.5}$$

Nevertheless, eq. (3.4) is only approximately correct: since the quadratic approximation to (3.3) is restricted to the region $\theta \ll 1$ it is not justified to require normalizability of ψ_0 for $\theta \gtrsim 1$. One therefore has to replace (3.4) by a combination of parabolic cylinder functions [29]:

$$\psi_0(z) = \frac{N}{2z}\left[D_\nu(z) - D_\nu(-z)\right]$$
$$z = \sqrt{2}\,\frac{2\theta}{g} \tag{3.6}$$

with energy eigenvalues $E = \nu + \frac{1}{2}$. For $\nu = 1$ this reduces to (3.4); for $\nu \neq$ positive integer the asymptotic behavior ($g \ll \theta \ll 1$) is:

$$\psi_0(z) = \frac{N}{2z}\left[z^\nu e^{-z^2/4} - (-z)^\nu e^{-z^2/4} - \frac{\sqrt{2\pi}}{\Gamma(1-\nu)} z^{-\nu-1} e^{z^2/4}\right] . \tag{3.7}$$

For ν close to one:

$$\psi_0(z) = \frac{N}{z}\left[z^\nu e^{-z^2/4} + \frac{1}{2}(1-\nu)\sqrt{2\pi}\, z^{-\nu-1} e^{z^2/4}\right] . \tag{3.8}$$

The main difference between (3.4) and (3.7) or (3.8) is the term $\sim e^{z^2/4}$: in addition to the exponentially decreasing term $e^{-z^2/4}$ there is also an exponentially increasing term $e^{z^2/4}$ which, in the semiclassical approximation, has necessarily to be present.

In the present problem it is most convenient to visualize the situation in the 3-dimensional phase space of the SU(2)-element U: it has the topology of S_3, and our quadratic approximation is valid on a 3-dimensional tangential plane at the north pole. We now choose Σ_0 to be a sphere around the north-pole with radius $g \ll \theta_0 \ll 1$. On the surface of this sphere we have $p_\theta = \frac{\partial S}{\partial \theta} = 4\theta$, $p_\vartheta = p_\varphi = 0$. With these starting conditions, the classical equations of motion to be solved reduce to

$$\ddot{\theta} = \sin\theta, \qquad \theta = 4\arctan(e^t) \tag{3.9}$$

$$S = \int_0^\theta d\theta' \sqrt{32(1-\cos\theta')} \sim \left\{ \begin{array}{ll} 2\theta^2 & (\theta \text{ small}) \\ 16 - 8(\pi-\theta) & (\theta \text{ near } \pi) \end{array} \right\} \tag{3.10}$$

with $\varphi \equiv$ const, $\vartheta \equiv$ const. Hence the classical trajectories are rays leaving the north pole at $t = -\infty$. Along any of these rays the first focal point is at the south pole of S_3 ($\theta = \pi$). According to what we have said in the previous section, the semiclassical approximation will be invalid near this focal point *). This can be deduced from the calculation of the prefactor from eq. (2.9). One finds:

$$\ln A^2 = -\left\{ \ln \sin\frac{\theta}{2} + 2\ln\sin\theta - 2E \ln \operatorname{tg}\frac{\theta}{4} \right\} + \ln N^2, \tag{3.11}$$

which implies

*) It also happens that at the south pole the metric of our coordinate system becomes singular ($g^{\theta\theta}=1$, $g^{\vartheta\vartheta} = 1/\sin^2\theta$, $g^{\varphi\varphi} = 1/\sin^2\theta\sin^2\vartheta$) . . This is, however, a feature of our choice of coordinates, and it should be distinguished from the appearance of the focal point.

$$A(\theta) \underset{\theta\to\pi}{\sim} \frac{N}{\pi-\theta} \tag{3.12}$$

near the south pole. (Similarly the north pole is an intersection point of different trajectories, A is singular also for $\theta \to 0$.)

We therefore return to the Schrödinger equation and demand that, away from the south pole, the solution matches the semiclassical approximation. If we approximate the potential in (3.3) by the constant value $8/g^2$, the Schrödinger equation becomes a free wave equation for spherically symmetric (euclidean) waves. A solution can therefore be written as a superposition of spherically symmetric rays:

$$\psi_0(\theta) = N' \int_0^\pi d\vartheta \cos\vartheta \int_0^{2\pi} d\varphi\, e^{-K\cos\vartheta}, \qquad K = \frac{8(\pi-\theta)}{g^2}$$
$$= (2\pi)^{3/2} N' \frac{I_{1/2}(z)}{\sqrt{z}} . \tag{3.13}$$

Alternatively, we could start from the Schrödinger equation ($\bar\theta = \pi - \theta$):

$$\left[-\frac{g^2}{8}\left(\frac{\partial^2}{\partial\bar\theta^2} + \frac{2}{\bar\theta}\frac{\partial}{\partial\bar\theta} \right) + \frac{8}{g^2} \right] \psi_0(\bar\theta) = E\,\psi_0(\bar\theta) \tag{3.14}$$

and pick the solution which is regular at $\bar\theta = 0$. The normalization in (3.13) has to be chosen such that it matches the semiclassical behavior (3.10), (3.11):

$$\psi_0(\theta) = N \frac{2^6\sqrt{\pi}}{g^2} e^{-16/g^2} \frac{I_{1/2}\left(\frac{8(\pi-\theta)}{g^2}\right)}{\sqrt{\frac{8(\pi-\theta)}{g^2}}} . \tag{3.15}$$

This solution exhibits all those characteristics which we have listed in the previous section:

(i) At the south pole $\theta = \pi$, ψ_0 takes the value

$$\psi_0(\pi) = N \frac{2^6\sqrt{2}}{g^2} e^{-16/g^2} . \tag{3.16}$$

It is, therefore, regular as a function of θ . Note that as a function of g^2 the prefactor goes as $O(g^{-2})$. Normalization is chosen such that for any point away from the south pole or the north pole the prefactor is independent of g.

(ii) Asymptotic behavor of $\psi_0(\theta)$ sets in for $g^2 \ll \pi - \theta$. In this region it matches the semiclassical approximation:

$$\psi_0(\theta) \sim N e^{-16/g^2} \frac{2^{5/2}}{\pi-\theta} \left[e^{8(\pi-\theta)/g^2} - e^{-8(\pi-\theta)/g^2} \right] . \qquad (3.17)$$

This has to be compared with (3.10) and (3.12): the "singularity" $\sim 1/(\pi-\theta)$ disappears if we take a closer look at distances $\pi-\theta = O(g^2)$ and use the full solution (3.15). The configuration space thus divides itself into the "inner" part $\pi-\theta < g^2$ where the semiclassical approximation is not good enough and an "cuter" part $\pi-\theta > g^2$ where this approximation provides an adequate description.

In addition to these features which are typical for a focal point, the asymptotic behavior (3.17) contains another piece of information. It is only the first term in the brackets of (3.17) which matches the semiclassical solution $\psi_0 = A \exp\left[-\frac{1}{g^2} S\right]$ with S of (3.10). We interpret it as a spherical wave whose center is located at the north pole. On its way towards the south pole it decreases exponentially. The second piece in (3.17) belongs to a wave which moves in the opposite direction. In terms of classical trajectories, the first piece belongs to classical solutions which at time $t = -\infty$ have left the north pole and at time $t = 0$ arrive at the south pole. In the second wave, the trajectories have traversed their common focal point and are on their way back to the north pole. Because of the rotational symmetry it is clear that the north pole is again a common focal point, and beyond this point

the whole procedure repeats itself. As a result, there is a whole tower of exponentially small contributions, and our discussion only refers to the leading two terms.

For this simple model it is not difficult to calculate even exponentially small corrections to the ground state energy. The exponentially small piece near the north pole comes from trajectories which have completed a full circle:

$$1-\nu = -\frac{1}{\sqrt{\pi}} 2^{11} g^{-3} e^{-32/g^2} . \qquad (3.18)$$

For further illustration, we consider in Appendix A another version of the one-plaquette model. There the ground-state is (almost) degenerate, and the splitting is exponentially small. The same kind of arguments which have led us to (3.18) can there be used to calculate the mass gap (A.8).

Although this one plaquette model has given us a first illustration of a focal point and its characteristics, it is far too simple and, if we would stop here, it would leave us a misleading impression. What it has shown correctly is that, because of the compactness of the configuration space, classical trajectories are likely to intersect. In the neighbourhood of a focal point, the wave function has certain distinctive peculiarities. Special to this model, however, are position and simplicity of the focal point: because of the symmetry, all trajectories intersect at the same point, the south pole. As we shall see, in a more general model the coupling between the plaquettes generates a much more sophisticated shape of the caustic, and some parts of it are considerably closer to the origin than the south pole. After the study of the two plaquette model we will have a clearer impression that caustics really are a dynamical effect.

We finally mention that the singularity of the function S of the one-plaquette model is not contained in Arnold's list of normal forms [22]: in our case we have a three-dimensional configuration space, and the singularity consists of an isolated point, the south pole. In Arnold's language, this singularity is not stable. The appearance of this unstable singularity is closely related to gauge invariance.

IV. Two-Plaquette Model

1. Model and computer analysis.

The Hamiltonian of this model is (Fig. 3):

$$H = -\frac{g^2}{8}\sum_{\ell=1}^{7}\Delta'_\ell + \frac{2}{g^2}\left\{ tr\left[1 - U_1^{-1}U_6U_5U_7^{-1}\right] + tr\left[1 - U_7U_4U_3^{-1}U_2^{-1}\right]\right\}. \tag{4.1}$$

Our treatment will be similar to that of the previous section. The gauge tree consists of all links but 4 and 5. Along the gauge tree we fix the link variables to unity and are left with two remaining loop variables $B_I = U_1^{-1}U_6U_5U_7^{-1}$ and $B_{II} = U_7U_4U_3^{-1}U_2^{-1}$. In terms of these variables the Hamiltonian becomes:

$$\begin{aligned} H = \frac{g^2}{2}\Big[4\,\vec{\mathcal{J}}_L^{\,2}(I) + 4\,\vec{\mathcal{J}}_L^{\,2}(II) - 2\,\vec{\mathcal{J}}_L(II)\cdot\vec{\mathcal{J}}_R(II)\Big] \\ + \frac{2}{g^2}\Big[\, 4 - tr\,B_I^{-1} - tr\,B_{II}^{-1}\,\Big] \,, \end{aligned} \tag{4.2}$$

where $\vec{\mathcal{J}}_{L,R}$ are the differential operators [16]

$$\vec{\mathcal{J}}_{L,R} = \frac{1}{2}\left[\mp\vec{L} + x_0\vec{P}\right], \quad \vec{P} = \frac{1}{i}\vec{\nabla}, \quad \vec{L} = \vec{x}\times\vec{P} \tag{4.3}$$

with $\vec{\mathcal{J}}_L^{\,2} = \vec{\mathcal{J}}_R^{\,2} = \Delta'$. In (4.3) the operators are written in cartesian coordinates. For later purposes it will also be useful to have them expressed in polar coordinates. By the chain rule one finds:

$$\begin{aligned} 2i\,\vec{\mathcal{J}}_{L,R} = & \begin{pmatrix} \cos\varphi & -\sin\varphi & 0 \\ \sin\varphi & \cos\varphi & 0 \\ 0 & 0 & 1 \end{pmatrix}\cdot\begin{pmatrix} \cos\vartheta & 0 & \sin\vartheta \\ 0 & 1 & 0 \\ -\sin\vartheta & 0 & \cos\vartheta \end{pmatrix}\cdot \\ & \begin{pmatrix} \cos\theta & \pm\sin\theta & 0 \\ \mp\sin\theta & \cos\theta & 0 \\ 0 & 0 & 1 \end{pmatrix}\cdot\begin{pmatrix} \frac{1}{\sin\theta} & 0 & 0 \\ 0 & \frac{1}{\sin\theta\sin\vartheta} & 0 \\ 0 & 0 & 1 \end{pmatrix}\cdot\begin{pmatrix} \frac{\partial}{\partial\vartheta} \\ \frac{\partial}{\partial\varphi} \\ \frac{\partial}{\partial\theta} \end{pmatrix}. \end{aligned} \tag{4.4}$$

Before rewriting (4.2) in terms of polar coordinates we note the following. After having exploited local gauge invariance in order to fix the link variables along the gauge tree, we still have the freedom of performing one global SU(2) rotation. Such a gauge transformation acts as a spatial rotation of the SU(2) vectors B_I and B_{II}. Therefore the gauge invariant ground state wave function can depend only upon the relative (spatial) angle between the vectors B_I and B_{II}. Among the remaining three angles, one of them belongs to a rotation of one of the B-vectors around the other. The other two parametrize rotations which rotate B_I and B_{II} simultaneously. It is therefore suggestive to define the two spatial angles ϑ_1 and φ_1 of B_I relative to a fixed coordinate system, whereas ϑ_2 and φ_2 are defined relative to the vector B_I. Since the wave function then will not depend upon ϑ_1, φ_1, and φ_2, these degrees of freedom must drop out of our problem. We demand that, as starting conditions for the classical trajectories near the origin, the momenta $p_{\vartheta_1}, p_{\varphi_1}, p_{\varphi_2}$ are zero. From the equation of motion it then follows that they remain zero forever, and the remaining equation of motion for the physical degrees of freedom ($\theta_1, \theta_2, \vartheta_2$ and their conjugate momenta) become independent of $\vartheta_1, \varphi_1, \varphi_2$ and their momenta. That means that $\vartheta_1, \varphi_1, \varphi_2$ still evolve as functions of time, but gauge invariant quantities do not depend upon them. Nevertheless, we shall come back to the rotations of φ_2.

Rather than presenting the Hamiltonian (4.2) in terms of polar coordinates, we immediately switch to classical mechanics. With the ansatz $\psi = A \cdot \exp[-\frac{1}{g^2} S]$ we arrive at the following classical Hamiltonian:

$$H = \frac{1}{8g^2}\Big[4 p_{\theta_1}^2 + 4 p_{\theta_2}^2 - 2 \cos\vartheta\, p_{\theta_1} \cdot p_{\theta_2} +$$

$$+ 4 p_\vartheta^2 \left(\frac{1}{\sin^2\theta_1} + \frac{1}{\sin^2\theta_2} \right) + 2 p_\vartheta^2 \frac{\cos\theta_1 \cos\theta_2 \cos\vartheta - \sin\theta_1 \sin\theta_2}{\sin\theta_1 \sin\theta_2}$$

$$+ 2 \sin\vartheta\, p_\vartheta \left(p_{\theta_1} \operatorname{ctg}\theta_2 + p_{\theta_2} \operatorname{ctg}\theta_1 \right) \Big]$$

$$+ \frac{4}{g^2} \left[2 - \cos\theta_1 - \cos\theta_2 \right] . \qquad (4.5)$$

Here we have set $p_{\vartheta_1} \equiv p_{\varphi_1} \equiv p_{\varphi_2} \equiv 0$ and relabelled $\vartheta_2 = \vartheta$. The equations of motion which follow from (4.5) are given in Appendix B.

As a first step we consider the quadratic approximation. The appropriate approximation to (4.2) is:

$$H = -\frac{1}{8} g^2 \left[4\Delta_1 + 4\Delta_2 - 2 \vec{\nabla}_1 \cdot \vec{\nabla}_2 \right] + \frac{2}{g^2} \left(\vec{x}_1^{\,2} + \vec{x}_2^{\,2} \right), \qquad (4.6)$$

where we have returned to cartesian coordinates. With $\vec{z}_{1,2} = \frac{1}{\sqrt{2}} (\vec{x}_1 \pm \vec{x}_2)$ H can be diagonalized, and the lowest energy wave function is:

$$\psi_0(\vec{x}_1, \vec{x}_2) = N \cdot \exp\left[-\frac{1}{g^2} S \right] \qquad (4.7)$$

$$S = 2 \left(\frac{\vec{z}_1^{\,2}}{\omega_1} + \frac{\vec{z}_2^{\,2}}{\omega_2} \right)$$

$$= \left(\frac{1}{\omega_1} + \frac{1}{\omega_2} \right) \left(\vec{x}_1^{\,2} + \vec{x}_2^{\,2} \right) + 2 \cdot \left(\frac{1}{\omega_1} - \frac{1}{\omega_2} \right) \vec{x}_1 \cdot \vec{x}_2 \qquad (4.8)$$

$$\omega_1^2 = 3 , \quad \omega_2^2 = 5 .$$

As mentioned before, S depends only upon $\theta_1^2 = \vec{x}_1^{\,2}$, $\theta_2^2 = \vec{x}_2^{\,2}$, and the relative angle ϑ

between $\vec{x}_1$ and $\vec{x}_2$. We can use S in (4.8) in order to define starting conditions for our classical trajectories. Then $p_{\vartheta_1} = \frac{\partial S}{\partial \vartheta_1} = 0$, $p_{\varphi_1} = \frac{\partial S}{\partial \varphi_1} = 0$, $p_{\varphi_2} = \frac{\partial S}{\partial \varphi_2} = 0$ whereas

$$p_{\theta_1} = \frac{\partial S}{\partial \theta_1} = 2\theta_1 \left(\frac{1}{\omega_1} + \frac{1}{\omega_2} \right) + 2\theta_2 \cos\vartheta \left(\frac{1}{\omega_1} - \frac{1}{\omega_2} \right), \qquad (4.9)$$

and similar expressions hold for p_{θ_2} and p_ϑ. It should be noted that in the same way as the gaussian approximation (3.4) represents the leading term of the parabolic cylinder function (3.6) - (3.8), the wave function (4.7), (4.8) is the dominant part of a more complicated expression. Eq. (4.7) describes an "outgoing" wave which exponentially decreases away from the origin. However, because of the compactness of the group manifold, part of this "outgoing" wave tunnels back to the origin and arrives as an "incoming" wave with an exponentially small amplitude. These exponentially small pieces have to be added to (4.7). From the point of view of harmonic oscillators, the Hamiltonian (4.6) after diagonalization describes two uncoupled oscillators, each of which can be treated in the same way is in section III. The true ground state wave function near the origin then is a product of the two single oscillator functions, but since there is freedom to distribute the full energy E between the two oscillators, the wave function really is a superposition of such product states. It is conceivable that a closed representation in terms of products of parabolic cylinder functions holds.

In the next step we solve the equations of motion derived from (4.5). Apart from the special case $\vartheta \equiv 0, p_\vartheta \equiv 0$, $\theta_1 \equiv \theta_2$, $p_{\theta_1} \equiv p_{\theta_2}$ no closed analytic solution is available. So we have used the computer (in Appendix B we describe a perturbation around a soluble case). The configuration space in which the classical solutions have to be visualized is 3-dimensional (θ_1, θ_2, and ϑ). There is the peculiarity that the boundary planes $\theta_1 = 0, \pi$ or $\theta_2 = 0, \pi$ have to

be contracted to a line: for example, on the plane $\theta_2 = 0$ points with the same value θ_1, but different ϑ are identical (Fig. 4). This whole plane should really be contracted into a single horizontal line (as we have indicated by arrows in Fig. 5). We further note that solutions in the horizontal plane $\vartheta = 0$ always stay in this plane; the same holds for the vertical plane $\theta_1 = \theta_2$. Finally, we should not forget about the other angle variables ϑ_1, φ_1, and φ_2 upon which the ground state wave function does not depend. Here φ_2 plays a special rôle in the following sense: if we rotate one of the loop variables B around the other, say B_{II} around B_I, then φ_2 changes, but all points in Fig. 4 with $\vartheta = 0$ are left invariant. This rotation in φ_2 will be of importance later on.

Rather than following the evolution in time of classical trajectories we concentrate directly on focal points. They are determined in the following manner. Let us return, for a moment, to the notation of section II. If $\bar{x}$ denotes the starting point for a classical trajectory x(t) (with starting value of momenta $\bar{p} = \frac{\partial S}{\partial x}\Big|_{x=\bar{x}}$), then choose N-1 other points close to $\bar{x}$, e.g.

$$\begin{array}{c} (\bar{x}_1 + \delta x_1, \bar{x}_2, \ldots, \bar{x}_N) \\ \cdots \\ (\bar{x}_1, \bar{x}_2, \ldots, \bar{x}_{N-1} + \delta x_{N-1}, \bar{x}_N). \end{array} \qquad (4.10)$$

The corresponding momenta are again obtained by differentiating S. Denote the corresponding trajectories by $x(t) + \delta x^{(i)}(t)$ (i = 1, ..., N-1). For finite time they will stay close to x(t), i.e. the deviations $\delta x^{(i)}(t)$ remain small. So we can linearize the equations of motion:

$$\delta \dot{x}^{(i)}(t) = \frac{\partial^2 H}{\partial x \partial p}\Big|_{\substack{x=x(t) \\ p=p(t)}} \cdot \delta x^{(i)}(t) + \frac{\partial^2 H}{\partial p \partial p}\Big|_{\substack{x=x(t) \\ p=p(t)}} \cdot \delta p^{(i)}(t) \qquad (4.11)$$

$$-\delta \dot{p}^{(i)}(t) = \frac{\partial^2 H}{\partial x \partial x}\Big|_{\substack{x=x(t) \\ p=p(t)}} \cdot \delta x^{(i)}(t) + \frac{\partial^2 H}{\partial p \partial x}\Big|_{\substack{x=x(t) \\ p=p(t)}} \cdot \delta p^{(i)}(t). \qquad (4.12)$$

A focal point is reached if at some time t our trajectory x(t) intersects with some neighboring trajectory which can be written as a linear combination of the $\delta x^{(i)}(t)$:

$$x(t+\delta t) = x(t) + \delta t \cdot \dot{x}(t) = x(t) + \sum_{i=1}^{N-1} \alpha_i \, \delta x^{(i)}(t) \; . \tag{4.13}$$

This can happen only if

$$0 = det \begin{pmatrix} \delta x_1^{(1)} & & \delta x_1^{(N-1)} & \dot{x}_1 \\ \vdots & \cdots & \vdots & \vdots \\ \delta x_N^{(1)} & & \delta x_N^{(N-1)} & \dot{x}_N \end{pmatrix} . \tag{4.14}$$

So for each classical trajectory x(t) we have to calculate N-1 other trajectories (by solving (4.11), (4.12)) as well as the determinant (4.14). In our two-plaquette model, N=3. We therefore need two more trajectories with starting values

$$(\bar{\theta}_1 + \delta\theta_1, \bar{\theta}_2, \vartheta) \qquad (\bar{\theta}_1, \bar{\theta}_2 + \delta\theta_2, \vartheta) \tag{4.15}$$

Starting values for the momenta are obtained by differentiating S in (4.8).

Let us now briefly describe the results of a computer analysis. We begin in the plane $\theta_1 = \theta_2$ and plot the lines of focal points (Fig. 5). They are obtained by varying the starting angle $\bar{\vartheta}$ near the origin and by then calculating, for each single trajectory x(t), the position of the first two focal points. The most interesting part of Fig. 5 are the cusp on the line $\vartheta = 0$ at $\theta_1 = \theta_2 \approx 2.39$ and the point F at $\theta_1 = \theta_2 \approx 2.645$, $\vartheta \approx 1.66$. The position of the

cusp has also been calculated analytically in Appendix B. In Fig. 6 we illustrate how classical trajectories behave in the vicinity of the cusp: the lines of focal points are envelopes to the classical trajectories. This holds everywhere on the left hand branch in Fig. 5, the branch on the right hand side is generated by trajetories which do not lie in the plane $\theta_1 = \theta_2$. Near the cusp in Fig. 6 we easily see that each point to the left of the lines of focal points is reached by only one trajectory; on the right hand side three different trajectories pass through each point.

Leaving the plane $\theta_1 = \theta_2$ we first follow the tip of the cusp. It always stays in the plane $\vartheta = 0$, and it describes a curve which is shown in Fig. 7. The embredding of the point F into the 3-dimensional $\theta_1, \theta_2, \vartheta$ space is indicated in Fig. 8. It looks like a bottle-neck, although the "bottle" above and below is triangle-shaped. Near any of the 3 corner lines we have a cusp-structure similar to that of Fig. 5. All smooth pieces of the 2-dimensional caustic are envelopes to classical trajectories. From this it follows that at the "bottle-neck" classical trajectories are squeezed together in order to pass through the point F in the $\theta_1 = \theta_2$ plane. Combination of Figs. 5-8 provides further information on the caustic Σ_f: above and below the bottle-neck the ends of the caustic Σ_f are tied to the corner points $(\theta_1, \theta_2, \vartheta) = (\pi,\pi,0) = (\pi,\pi,\pi)$, $(\pi,0,0) = (\pi,0,\pi)$, $(0,\pi,0) = (0,\pi,\pi)$ and the origin. These points are then singular, too. The fact that Σ_f also reaches the origin relates back to our discussion after (4.9): there is not only an "incoming" wave front which reaches the origin, but from a particular direction $(\vartheta = \pi)$ this wave front is even singular. Altogether we see that the caustic is a rather involved 2-dimensional surface with corners, cusps and the bottle-neck. Intuitively one may think that these one or zero dimensional parts of Σ_f are more singular than the smooth pieces, and the wave function will be

more singular than elsewhere. We shall see that this is more or less correct.

There is still another part of the caustic which does not require further computing work. Combination of Figs. 5 and 6 shows that trajectories which leave the origin with some $\bar{\vartheta} > 0$ eventually come down again and pierce through the plane $\vartheta = 0$ at some point beyond the line of focal points shown in Fig. 7. In fact, each point of this part of the $\vartheta = 0$ plane is reached by such a trajectory coming from the origin. Now we have to remember that we still have the rotations in φ_2 which leave all the points of the plane $\vartheta = 0$ invariant. Each point in this plane, which can be connected with the origin through some trajectory x(t), can also be connected through a φ_2-rotated version of this trajectory and, hence, is a focal point on x(t). This implies that the whole plane $\vartheta = 0$ beyond the line shown in Fig. 7 is part of the caustic. As we shall discuss below, it turns out that this is the most singular part of the caustic.

2. The cusp singularity

In the following we shall describe how the wave function behaves in the neighbourhood of the most singular parts of the caustic. We start with the cusp in the $\theta_1 = \theta_2$ plane and ignore the direction perpendicular to this plane, since this dimension does not participate in building up the singularity. Our construction goes in various steps: we start from Arnold's list [20] of normal forms of S, then construct a solution to the Schrödinger equation which away from the cusp matches the semiclassical approximation, and, finally, include the φ_2-rotation. All this will first be done in the classically allowed region, then translated into our situation of the two-plaquette model where all this structure lies in the forbidden region.

As we have outlined in Section II, the singularities which one encounters in a semiclassical analysis are singularities of the projection map in 2n-dimensional pq-space of the n-dimensional manifold $\{ p,q \mid q = \frac{\partial \mathcal{F}}{\partial p} \}$ onto the configuration q-space. According to Arnold [20], the cusp-singularity is described by the normal form:

$$\mathcal{F}(p_1, q_2) = p_1^4 + q_2 p_1^2 \tag{4.16}$$

with

$$q_1 = \frac{\partial \mathcal{F}}{\partial p_1} = 4 p_1^3 + 2 q_2 p_1 \tag{4.17}$$

$$p_2 = -\frac{\partial \mathcal{F}}{\partial q_2} = -p_1^2 \,. \tag{4.18}$$

In 4-dimensional (p_1, p_2, q_1, q_2)-space this describes a projection onto the q_1-q_2 plane. (4.17) is a cubic equation which can be solved analytically. A singularity of this mapping occurs if the Jacobian vanishes. In our case:

$$0 = \frac{\partial q_1}{\partial p_1} = 12 p_1^2 + 2 q_2 \,. \tag{4.19}$$

In the $q_1 q_2$-plane this describes the singular line

$$q_1 = \pm 8 \left(-\frac{q_2}{6} \right)^{3/2} , \tag{4.20}$$

which is illustrated in Fig. 9. Inside the shaded region the map has three preimages (i.e. three classical trajectories with different momenta reach a point in this region):

$$(p_1)_1 = 2\sqrt{-\frac{q_2}{6}}\,, \quad (p_1)_2 = -2\sqrt{-\frac{q_2}{6}}\cdot\cos\left(\frac{\varphi}{3}+60°\right)$$
$$(p_1)_3 = -2\sqrt{-\frac{q_2}{6}}\cdot\cos\left(\frac{\varphi}{3}-60°\right) \qquad (4.21)$$

with
$$\cos\varphi = \frac{q_1}{8\sqrt{-\frac{q_2}{6}}^3}\,. \qquad (4.22)$$

Outside this region there is only one (real) solution with an expression similar to (4.21), (4.22). Clearly, this type of singularity looks very much the same as the cusp in Fig. 5.

A more detailed analysis, however, shows that the singularity structure of (4.16) does not yet in all detail agree with the result of our computer study. What is not yet right is the shape of classical trajectories whose slope p_2/p_1 can be calculated from (4.21) and (4.18): they are not tangent to the singular line (4.20), whereas in Figs. 5 and 6 the singular line is the envelope of the classical trajectories. On the other hand we know from the discussion in Ref. 20 that the normal form (4.16) always allows for a smooth change of variables which leaves the shape of the singular lines invariant. We could now try to construct this transformation of coordinates; however, it turns out to be much more convenient to proceed directly to the next step of our task, namely the construction of a solution to the Schrödinger equation in the vicinity of the cusp. This will give us the desired function $S(q_1,q_2)$ from which we can read off the necessary change of variables in (4.16).

In order to illustrate the general idea we return to the notation of Section II and work in a classically allowed region. The task is to solve the Schrödinger equation

$$\left[-\hbar^2\Delta - k_0^2\right]\psi(q_1,q_2) = 0 \qquad (4.23)$$

with the requirement that, away from the point $(q_1,q_2) = (0,0)$ the limit leads to a wave function of the form $\psi(q_1,q_2) \sim A(q_1,q_2)\exp\left[\frac{i}{\hbar}S(q_1,q_2)\right]$ with S showing the characteristics of Figs. 5 and 6. Clearly, any superposition of plane waves $\exp\left[\frac{i}{\hbar}\vec{p}\cdot\vec{q}\right]$ with $\vec{p}^{\,2} = k_0^2$ is a solution of (4.23). The direction of the classical trajectories in Fig. 6 suggests that the momentum $\vec{p}$ is mainly along the 2-direction, i.e. $|p_1| \ll |p_2|$. In this approximation we write:

$$\psi(q_1,q_2) = \int dp_1\, \exp\left[\frac{i}{\hbar}\left(q_1p_1 + k_0q_2 - \frac{p_1^2}{2k_0}q_2\right)\right]\cdot f(p_1)\,. \qquad (4.24)$$

Comparison with (4.16) shows that the ansatz

$$f(p_1) = \exp\left[-\frac{i}{\hbar}p_1^4\right] \qquad (4.25)$$

satisfies all our demands. The exponent in (4.24) becomes:

$$S = q_1p_1 + k_0q_2 - \frac{p_1^2}{2k_0}q_2 - p_1^4\,. \qquad (4.26)$$

In (4.23) we can always rescale the q's such that $k_0 = \frac{1}{2}$. Then:

$$S = q_1p_1 + \tfrac{1}{2}q_2 - p_1^2q_1 - p_1^4\,. \qquad (4.27)$$

In the limit $\hbar \to 0$ the integral in (4.24) is evaluated by means of the saddle point method. The condition for the existence of an extremum is:

$$0 = \frac{\partial S}{\partial p_1} = q_1 - \frac{\partial}{\partial p_1}\left(p_1^2q_2 + p_1^4\right)\,. \qquad (4.28)$$

This agrees with (4.16), (4.17) and, hence, in the q_1-q_2 plane the line of singularities is the same as (4.20). Only the value of p_2 is slightly changed:

$$p_2 = \frac{\partial S}{\partial q_2} = \frac{1}{2} - p_1^2 \quad . \tag{4.29}$$

This has to be compared with (4.18): it is this change of p_2 which, near the tip of the cusp, makes the trajectories tangent to the line of singularities. To finish the discussion of (4.24), (4.25) we still have to calculate the fluctuations around the saddle point. It yields the prefactor A:

$$A = \int dp_1 \, e^{i/2\hbar \cdot (p_1 - p_{1\,saddle})^2 \cdot S''} = \sqrt{\frac{2\pi i \hbar}{S''}} \, . \tag{4.30}$$

It is well defined unless

$$S'' = -12 p_1^2 - 2q_2 = 0 \, . \tag{4.31}$$

This is just the defining equation of the singular line (4.19), (4.20). On this line we cannot use the gaussian approximation (4.30) but have to keep higher than quadratic terms in S. The result is still well-defined, but relative to a regular contribution (4.30) it goes as $\hbar^{-1/6}$. An exception to this is the tip of the cusp, the point $(q_1,q_2) = (0,0)$. There we use directly (4.24) and find that the prefactor diverges $\sim \hbar^{-1/4}$ relative to a regular contribution with $S'' \neq 0$. So the tip of the cusp is more singular than the singular lines.

Next we try to incorporate the extra degree of freedom which corresponds to rotations in φ_2. In terms of those variables which we are using presently, we are looking for a solution which is invariant under rotation around the q_2-axis. As a result of this, the negative q_2-axis should become part of the caustic. It is not difficult to find the appropriate generalization of eq. (4.24). Let simply $\vec{p}_1 = (p_{11}, p_{12})$ and $\vec{q}_1 = (q_{11}, q_{12})$ be two dimensional vectors. Then (4.24) becomes:

$$\psi(q_1,q_2) = \int\limits_{|\vec{p}_1| \ll \frac{1}{2}} d^2 p_1 \, \exp\left[\frac{i}{\hbar}\left(\vec{q}_1 \vec{p}_1 + \tfrac{1}{2} q_2 - q_2 \vec{p}_1^{\,2} - (\vec{p}_1^{\,2})^2\right)\right] . \tag{4.32}$$

Call this exponent again S and repeat the same steps done before. The saddle point conditions are:

$$\begin{aligned} 0 &= \frac{\partial S}{\partial p_{11}} = q_{11} - 4 p_{11}\left(p_{11}^2 + p_{12}^2\right) - 2 q_2 p_{11} \\ 0 &= \frac{\partial S}{\partial p_{12}} = q_{12} - 4 p_{12}\left(p_{11}^2 + p_{12}^2\right) - 2 q_2 p_{12} \, . \end{aligned} \tag{4.33}$$

The caustic is defined by the condition that, in addition to the first derivatives in (4.33), the determinant of the matrix of second derivatives of S vanishes:

$$0 = \left(p_{11}^2 + p_{12}^2 + \frac{q_2}{2}\right)\left(3 p_{11}^2 + 3 p_{12}^2 + \frac{q_2}{2}\right) . \tag{4.34}$$

Solutions to (4.33) and (4.34) fall into two classes: either

$$q_2 \leq 0 \, , \quad \vec{q}_1 = 0 \, , \quad \vec{p}_1^{\,2} = -\frac{q_2}{2} \tag{4.35}$$

or

$$q_2 < 0 \, , \quad |\vec{q}_1| = 8\sqrt{-\frac{q_2}{6}} \, , \quad |\vec{p}_1| = \sqrt{-\frac{q_2}{6}} \, , \quad \vec{p}_1 \parallel \vec{q}_1 \, . \tag{4.36}$$

The first solution is the negative q_2-axis, the second solution represents the rotationally invariant generalization of the previous singular line (4.20). As to the singular behavior in the limit $\hbar \to 0$ we find, after some algebra, the following behavior (relative to a regular point). On the line (4.35), which includes the tip of the cusp at the origin, A diverges as $\hbar^{-1/2}$. On the surface (4.36) still A $\sim \hbar^{-1/6}$, just as before. We see that, as a result of the additional rotational degree of freedom, not only has the caustic received an additional piece, but this new piece is also the most singular part of the caustic.

Finally we have to take care of the fact that, in our two-plaquette model, the caustic lies in the classically forbidden region. The analogue of (4.24) is:

$$\psi(q_1,q_2) = \int_{|p_1|\ll|p_2|} dp_1 \exp\left[\frac{1}{g^2}\left(p_1 q_1 + \tfrac{1}{2} q_2 - p_1^2 q_2 - p_1^4\right)\right]. \tag{4.37}$$

In contrast to the oscillatory case considered before we now no longer look for stationary points in the exponent but for maxima. A closer look at the second derivative shows that outside the shaded region in Fig. 9 we have one maximum (as in the oscillatory case we had one stationary point), whereas inside we have two maxima and one minimum. On the negative q_2-axis the two maxima have the same height. If we approach the singular line, the smaller of the two maxima combines with the minimum in order to form a saddle point and this disappears. So in contrast to the oscillatory case the wave function is no longer singular on the line of Fig. 9. It is only at the tip of the cusp that A still diverges: A $\sim \hbar^{-1/4}$ relative to a regular contribution. Similarly, if we apply the same argument to the analogue of (4.32), we find that the wave function is no longer singular on (4.36), but on the negative q_2-axis A still diverges as $\hbar^{-1/2}$ (relative to a regular point).

3. The bottle-neck singularity

We now return to the other singularity, the bottle-neck in Fig. 8, and perform a similar analysis. We again begin with Arnold's normal form [20] which applies to this case:

$$\mathcal{F} = p_1^2 p_2 - p_2^3 + q_3 p_2^2 \tag{4.38}$$

$$q_1 = \frac{\partial \mathcal{F}}{\partial p_1} = 2 p_1 p_2 \tag{4.39}$$

$$q_2 = \frac{\partial \mathcal{F}}{\partial p_2} = p_1^2 - 3 p_2^2 + 2 q_3 p_2 \tag{4.40}$$

$$p_3 = -\frac{\partial \mathcal{F}}{\partial q_3} = -p_2^2 . \tag{4.41}$$

In the six-dimensional $(q_1,q_2,q_3,p_1,p_2,p_3)$-space it describes a map onto the three-dimensional (q_1,q_2,q_3) subspace. The caustic is defined as the locus of singularities of this map: in addition to (4.39) - (4.41) we require that the Jacobian of the map $(p_1,p_2) \to (q_1,q_2)$ be singular:

$$0 = \frac{\partial(q_1,q_2)}{\partial(p_1,p_2)} = 4\left[p_2(-3p_2+q_3) - p_1^2\right]. \tag{4.42}$$

In the (q_1,q_2,q_3)-space, eqs. (4.39), (4.40), (4.42) describe a two-dimensional surface which is illustrated in Fig. 10. The main features of the result of our computer analysis (Fig. 8) are well reproduced. A little algebra shows that inside the "bottle-neck" the mapping has four preimages, outside there are only two. However, just as in the previous case, Arnold's normal form (4.38) is not yet exactly what we need. Again the trajectories whose slope can be calculated from (4.39) - (4.41) are not tangent to the caustic, and we have to make a change of variables. Again it is convenient to proceed directly to the next step of our analysis, the construction of the wave function near this singularity at $(q_1,q_2,q_3) = (0,0,0)$. We have to solve

$$\left[-\hbar^2\Delta - k_0^2\right]\psi(q_1,q_2,q_3) = 0 \tag{4.43}$$

such that for $\vec{q} \neq 0$ $\psi(q_1,q_2,q_3)$ in the limit $\hbar \to 0$ matches the semi-classical approximation. Starting from a superposition of plane waves with $|\vec{p}| = k_0$ we make the assumption that $\vec{p}$ is mainly along the q_3-axis. Then:

$$\vec{p}\cdot\vec{q} \sim p_1 q_1 + p_2 q_2 + p q_3 - \frac{q_3}{2p}\,(p_1^2 + p_2^2). \tag{4.44}$$

With p = 2 and a weight factor $\exp\left[\frac{i}{\hbar}(p_3^2 - p_1^2 p_2)\right]$ we obtain:

$$\psi(q_1,q_2,q_3) = \int_{|p_1|,|p_2|<<2} dp_1 dp_2 \exp\left[\frac{i}{\hbar}\left(\vec{p}\cdot\vec{q} + p_3^2 - p_1^2 p_2\right)\right]. \tag{4.45}$$

The exponent

$$S = p_1 q_1 + p_2 q_2 + 2q_3 - \frac{q_3}{4}(p_1^2 + p_2^2) + p_2^3 - p_1^2 p_2 \tag{4.46}$$

yields the saddle point conditions:

$$q_1 = 2p_1 p_2 + \tfrac{1}{2} p_1 q_3 \tag{4.47}$$

$$q_2 = \tfrac{1}{2} q_3 p_2 - 3p_2^2 + p_1^2 . \tag{4.48}$$

These equations coincide with (4.39), (4.40) if we put $p_2 \to p_2 - \frac{1}{4} q_3$ and restrict ourselves to small $q_3 << 1$ (disregard terms of order q_3^2). Therefore, the shape of the caustic in (q_1,q_2,q_3) -space is slightly deformed, but all the essential features (corner lines, bottle-neck, number of preimages) remain unchanged.

From (4.45), (4.46) we can read off the asymptotic behavior in the limit $\hbar \to 0$. Away from the caustic we have $\frac{\partial(q_1,q_2)}{\partial(p_1,p_2)} \neq 0$ and hence can use the method of stationary phase. If the point lies in the interior of the caustic we have four values (p_1,p_2) for which the exponent S is stationary, i.e. the wave function comes as a sum of four terms. For each of them, the gaussian fluctuations go as $O(\hbar)$. On the caustic we have to distinguish between the planar pieces and the corner lines. On the planar part the matrix of second derivatives $\frac{\partial^2 S}{\partial p_i \partial p_j}$

has one zero eigenvalue, and for the corresponding eigenvector the first nonvanishing term in the Taylor expansion of S is the cubic term. Appropriate scaling of the integration variables yields $A = O(\hbar^{1/2+1/3})$, i.e. relative to a regular point the prefactor goes as $\hbar^{-1/6}$. On the corner lines (except for the point $\vec{q} = 0$) there still is only one zero eigenvalue, but now the cubic term in the Taylor expansion of the exponent vanishes. So the first nonvanishing term is a mixed third derivative, as a result of which the integration variables have to be scaled differently. One finds $A = O(\hbar^{3/4})$, i.e. relative to a regular point the prefactor diverges as $\hbar^{-1/4}$. Finally, at $\vec{q} = 0$ we see from (5.45), (4.46) that $A = O(\hbar^{2/3})$, which means A diverges as $\hbar^{-1/3}$ compared to a regular point. So $\vec{q} = 0$ is the point of strongest divergence.

Strictly speaking this analysis is still incomplete for the following reason. So far we have constructed a solution to the Schrödinger equation which, in the vicinity of the most singular point $\vec{q} = 0$ (or the point F in Fig. 5) reproduces the singularity structure of our computer analysis. As we have mentioned earlier, each point inside the bottle-neck can be reached by four classical trajectories, each point outside by only two. Comparing this with the situation illustrated in Fig. 5 we notice that all trajectories come from above, i.e. they leave the origin with some initial $\vartheta > 0$ and eventually turn downwards *). There is , however, still another possibility to connect such a point with the origin: there is always a trajectory which leaves the origin with some $\vartheta < 0$. This then implies that our solution (4.45) cannot be complete because it does not contain this extra solution. But since these extra trajectories do not participate in building up the caustic near the bottle-neck, one may expect that they simply add an extra term to (4.45) and hence do not affect our conclusions.

*) For an interior point in the plane $\theta_1 = \theta_2$ above the bottle-neck F, two trajectories lie inside the plane $\theta_1 = \theta_2$ and two other trajectories pierce through this plane.

As the last step we have to replace $\hbar \to g^2$ and to locate our caustic into the classically forbidden region. From the previous example we have learned that only those stationary points of the exponent have a chance to survive as an identifiable term of the wave function which are genuine extrema and not just saddle points. A closer look at (4.39), (4.40), and the matrix of second derivatives $\frac{\partial^2 S}{\partial q_i \partial q_j}$ shows that there is altogether only one extremum inside the bottle-neck. For $q_3 > 0$ it is a maximum, for $q_3 < 0$ a minimum. All other stationary points turn out to be saddle points. It is now useful to connect our analysis of the vicinity of the bottle-neck with that of the cusp (Fig. 5): let us follow the path shown in Fig. 11. Near the cusp there is a well-defined term in the wave function ψ , until the trajectory reaches the plane $\vartheta = 0$. At this point there is a second, equal contribution from the "mirror" trajectory below the plane $\vartheta = 0$. Continuing along the classical path into the region $\vartheta < 0$, the corresponding contribution to ψ becomes subdominant to that of the "mirror" trajectory, but it still provides a well-defined term in the wave function since it belongs to a maximum of the exponent. This remains so until the trajectory hits some part of the caustic: from then on the extremum of the exponent turns into a saddle point. In this way each point inside the shaded region above the bottle-neck can be reached by one such trajectory, which agrees with our analysis of the vicinity of the bottle-neck. There is , of course, always the other trajectory which leaves the origin at $\vartheta < 0$ and always provides the dominant term to the wave function. In contrast to the analysis of the cusp singularity it is not possible to read these results directly off from the analytic continuation of (4.45); when replacing $i/\hbar$ by $-1/g^2$, the integral diverges for large p_2. If we introduce a cutoff, the main contribution will come from some endpoint of the integration. This difficulty reflects that (4.45) is incomplete: it does not contain the extra classical trajectory which, in fact, now even gives the dominant contribution.

4. A few additional remarks

This completes our presentation of results of the two plaquette model. As we have indicated before, this is still far from an exhaustive discussion of the ground state wave function. Along each classical trajectory which leaves the origin we have computed so far only the first two focal points. They form that part of the caustic which we have tried to illustrate. If we move further along any of these trajectories there are more focal points which are part of other pieces of the caustic. It is only because on these parts of the caustic the wave function is exponentially further suppressed that we stopped after the second focal point. Altogether our analysis suggests that for any point in configuration space the wave function is a sum of separate pieces; on the caustic some of these pieces coalesce and produce, in the limit $g^2 \to 0$, an additional negative power of g. Although far from being trivial, it appears to be possible to construct the wave function in the vicinity of the most interesting parts of the caustic. As a technical point it is apparently easier to perform the analysis of the wave function on a caustic in a classically allowed region; some of the structure then disappears when translating into the classically forbidden region.

The following remark may be very important. Clearly, our SU(2) two-plaquette model contains an analogous U(1) two-plaquette model: we only have to restrict our plaquette variables B_I and B_{II} to a U(1) subgroup ($\varphi_1 = \varphi_2 = 0$, $\vartheta_1 = 0$, $\vartheta_2 = 0$ or π) . It is interesting to note that in this restricted configuration space there is no caustic. In other words, intersections of neighboring trajectories only occur if we leave the U(1)-part of our configuration space. On the other hand, we have seen that the most singular part of the caustic is the plane $\vartheta = 0$ (beyond the line in Fig. 7), i.e. it lies in the U(1)-subspace. It is tempting to speculate that some of this will generalize to larger lattice models. If so, this represents a qualitative difference between abelian and non-abelian gauge theories.

V. Conclusions

In this paper we have started an investigation of the ground state wave function of nonabelian lattice gauge theories in the weak coupling limit. In this regime it seems natural to apply the semiclassical approximation which reduces the Schrödinger equation to a problem of classical mechanics. In this first part we have concentrated on a particular phenomenon, the caustics, which appear at some finite distance away from the origin. As the most prominent feature of caustics, the ground state wave function peaks as $g^{-p} e^{-\frac{1}{g^2} S}$ where the power p depends upon the detailed shape of the caustic. In order to illustrate this phenomenon in some detail we have chosen to study two simple models, one with only one SU(2) group element, the other one with two group elements. For these two examples, we have shown what the caustics are and how the wave function behaves in the vicinity of the caustic. It is not yet clear to us what, in a larger lattice model, the relevance of the caustics will be for confinement dynamics. We feel, however, tempted to speculate that, when we come to evaluate in a larger lattice model quantities of physical interest (vacuum expectation values of gauge invariant operators, time-time correlation functions etc.), the enhancement of the ground state wave function on the caustics gives a significant contribution.

Several remarks are in place concerning the interpretation of our results. First one may ask whether the caustics are merely an artifact of the simple models that we have selected or whether they are more general. We firmly believe that they are a general feature of nonabelian lattice models, and, as a support for this, we have started a computer analysis of a less naive lattice model, a cube of unit length. Again we have chosen free boundary conditions, as a result of which the Hamiltonian depends upon 7 SU(2)-group elements (after the usual procedure of gauge fixing). Results are encouraging in two respects: a) focal points

do exist and b) they are closer to the origin than in the two-plaquette model. We feel tempted to speculate that in larger lattice models they move even closer to the origin and may become accessible to some kind of analytic treatment.

Secondly, the appearance of caustics seems to be connected with the nonabelian nature of our lattice model. As we have pointed out at the end of Section IV, no caustic is found if we restrict ourselves to the U(1)-part of the configuration space $(\varphi_1 = \varphi_2 = 0,\ \vartheta_1 = 0,\ \vartheta_2 = 0 \text{ or } \pi)$. In order to have caustics we apparently need the freedom to leave the U(1)-part *). On the other hand, the most singular part of the caustic lies in U(1)-subspace: this is because this part of configuration space is left invariant under a special set of gauge transformation, namely the rotations in φ_2. Since this argument can easily be generalized to larger lattice models, we may speculate that this enhancement of the U(1)-part of field configurations will be more general, too.

We conclude with a few words on future steps of this program. Clearly the next most obvious task is to locate caustics in larger lattice models and to determine the behavior of the wave function in their vicinity. Taking an optimistic point of view one may hope that caustics will exist already in the region of small fields. One then might try to use some kind of perturbation theory for solving classical equations of motion. It will only be after knowing the caustics in some detail for a large lattice model that we can hope to understand which

---

*) This does not necessarily imply that compact QED has no caustics at all: for a complete analysis of the ground state wave function we have to follow the classical trajectories beyond the region $|\theta_1| < \pi,\ |\theta_2| < \pi$. All we can say is that, if caustics exist, they lie outside the region $|\theta_1| < \pi$, $|\theta_2| < \pi$, i.e. at much larger distances from the origin than in the nonabelian case.

rôle the caustics play in the dynamics of confinement. It may very well turn out that we also will have to explore the behavior of classical solutions at times long after they have left the origin. In the compact group space classical trajectories will circle around, and some of them will come back into the neighbourhood of the origin. After a while some regular pattern of motion may emerge which could be of importance. Altogether we feel that the applitation of modern methods of classical mechanics provides a promising tool for studying the weak coupling limit of lattice gauge theory models.

Acknowledgements

We are indebted to Professor John Bronzan for helpful discussions. One of us (TTW) wishes to thank Professor Hans Joos, Professor Harry Lehmann, Professor Roberto Peccei, Professor Paul Söding and Professor Volker Soergel for their kind hospitality at DESY. He is also grateful to the Alexander von Humboldt Foundation for a Humboldt Award.

Appendix A

In Section III, the one-plaquette case with free boundary is found to reduce to a one-dimensional problem after using gauge fixing and overall SU(2) gauge rotation. If the same procedures is applied to the one-plaquette case with periodic boundary condition (i.e., $U_1 = U_3$ and $U_2 = U_4$ with reference to Fig. 2), three variables remain. Thus the one-plaquette case with periodic boundary is roughly comparable in complexity with the two-plaquette case with free boundary.

In this Appendix, we discuss briefly another one-plaqutte case that reduces to a one-dimensional problem. The boundary conditions are chosen to be

$$U_1 = U_3^{-1} \quad \text{and} \quad U_2 = U_4^{-1}. \tag{A.1}$$

With these boundary conditions, the magnetic energy is, from (3.1),

$$V = \frac{2}{g^2} \, tr \, [1 - U_1 U_2 U_1 U_2]. \tag{A.2}$$

This is invariant under the gauge transformation

$$U_1 \to A U_1 B \quad \text{and} \quad U_2 \to B^{-1} U_2 A^{-1}, \tag{A.3}$$

where A and B are arbitrary elements of SU(2). If U_2 is put on the gauge tree, then only one variable is left. Using the variables of Section III the result is

$$V = \frac{4}{g^2} \, (1 - \cos 2\theta). \tag{A.4}$$

This differs from the corresponding V of Section III, e.g. (3.3), by merely the factor of 2 with θ.

This factor of 2 makes an important difference. While for free boundary V = 0 only at $\theta = 0$, for the present case V = 0 at both $\theta = 0$ and $\theta = \pi$. These two points, 0 and π, are distinct in the sense that they cannot be transformed into each other by (A.3). Consequently, unlike that of Section III the ground-state wave function is symmetrical under

$$\theta \to \pi - \theta \,. \tag{A.5}$$

There is an excited state, with exponentially small excitation energy $E_1 - E_0$, which is anti-symmetrical under (A.5).

There is some arbitrariness in choosing the electric energy. A natural choice is

$$T = \frac{g^2}{2}\left[\vec{g}^2(u_1) + \vec{g}^2(u_2) + \vec{g}^2(u_3) + \vec{g}^2(u_4)\right]. \tag{A.6}$$

With this choice, the Hamiltonian is

$$H = -\tfrac{1}{2}g^2\left(\frac{\partial^2}{\partial\theta^2} + 2\operatorname{ctg}\theta\frac{\partial}{\partial\theta}\right) + \frac{4}{g^2}(1-\cos 2\theta)\,. \tag{A.7}$$

The electric part agrees with that of Section III. If we argue that U_3 and U_4 are really not distinct from U_1 and U_2, then the electric part is simply

$$\frac{g^2}{2}\left[\vec{g}^2(u_1) + \vec{g}^2(u_2)\right],$$

which is half of the T of (A.6). Some rescaling with $2^{1/4}$ is then needed.

Following exatly the same procedure as that of Section III, the ground state energy E_0 and the energy E_1 of the first excited state are found to be

$$E_{0,1} = 6 - \frac{g^2}{2} \mp 2^{10}\pi^{-1/2} g^{-3} e^{-16/g^2}\,. \tag{A.8}$$

where the upper (lower) sign is for $E_0(E_1)$. Therefore the excitation energy is

$$E_1 - E_0 \sim 2^{11}\pi^{-1/2} g^{-3} e^{-16/g^2}\,. \tag{A.9}$$

A purist may question the meaning of the second term in the right-hand side of (A.8). After all, there are also corrections in powers of g^2. In contrast (A.9) has a rigorous meaning: it is an asymptotic expression in the sense of Poincaré for $g \to 0$.

Throughout this paper, we have concentrated on the very simplest cases of two-dimensional lattices. It is interesting to note that the present case has a natural extension to the cube, as shown in Fig. 12. The generalization of the boundary conditions (A.1) is

$$\begin{aligned} U_1 = U_4 = U_7^{-1} = U_{10}^{-1} \\ U_2 = U_5 = U_8^{-1} = U_{11}^{-1} \\ U_3 = U_6 = U_9^{-1} = U_{12}^{-1} \end{aligned} \tag{A.10}$$

The Hamiltonian is invariant under

$$U_i \to A\,U_i\,B\,, \tag{A.11}$$

where i = 1, 2, 3 and A, B are arbitrary elements of SU(2). Therefore, after gauge fixing and overall gauge rotation, three independent variables remain. This problem

of the cube is roughly comparable in complexity with, but has a larger discrete group of symmetry then, the two-plaquette problem of Section IV. Indeed, the electric part is essentially the T of (B.3) with

$$\alpha = \frac{1}{2} \ . \tag{A.12}$$

The corresponding V is zero at the following four points:

$$U_1 = U_2 = U_3 = 1$$

$$U_1 = -1 \ , \quad U_2 = U_3 = 1$$

$$U_2 = -1 \ , \quad U_3 = U_1 = 1$$

and $$U_3 = -1 \ , \quad U_1 = U_2 = 1 \ . \tag{A.13}$$

These four points are distinct in the sense that they cannot be transformed into each other by (A.11), which is the most general gauge transformation. There are therefore three linearly independent excited states with exponentially small excitation energy.

Appendix B

For the two-plaquette problem studied in Section IV, one of the most symmetric points of the caustic is the tip of the cusp in Fig. 5. This point is characterized by $\theta_1 = \theta_2$ and $\vartheta = 0$. It is the purpose of this Appendix to show that it is located at

$$\theta_1 = \theta_2 \sim 2.388704014 \ . \tag{B.1}$$

In terms of the variables $\theta_1, \theta_2,$ and ϑ together with their conjugate momenta $p_{\theta_1}, p_{\theta_2}$, and p_ϑ, the Hamiltonian is given by (4.5). It is convenient to generalize (4.5) slightly in the form

$$H = T + V \ , \tag{B.2}$$

where

$$T = \tfrac{1}{2} g^{-2} \Big[p_{\theta_1}^2 + p_{\theta_2}^2 - 2\alpha p_{\theta_1} p_{\theta_2} \cos\vartheta + p_\vartheta^2 \Big(\frac{1}{\sin^2\theta_1} + \frac{1}{\sin^2\theta_2} \Big)$$

$$+ 2\alpha p_\vartheta^2 \frac{1}{\sin\theta_1 \sin\theta_2} \big(\cos\theta_1 \cos\theta_2 \cos\vartheta - \sin\theta_1 \sin\theta_2 \big) \tag{B.3}$$

$$+ 2\alpha p_\vartheta \sin\vartheta \, \big(p_{\theta_1} \operatorname{ctg}\theta_2 + p_{\theta_2} \operatorname{ctg}\theta_1 \big) \Big]$$

and

$$V = 4 g^{-2} \big(2 - \cos\theta_1 - \cos\theta_2 \big) . \tag{B.4}$$

When

$$\alpha = \frac{1}{4} \tag{B.5}$$

this Hamiltonian reduces to that of (4.5). This factor of $\frac{1}{4}$ is due to the fact that there is one common link (7 of Fig. 3) out of the four links of each plaquette.

The classical trajectories of interest are all in the classically forbidden region. Thus the rapidly varying exponential factor is $\exp(-g^{-2}S)$; see eq. (2.3) and the last sentence of Section II. Another way of describing this situation is to say that the time in the classical equations of motion is purely imaginary. This purely imaginary time is conveniently avoided by reversing the sign of V. We therefore start with the Hamiltonian

$$T - V \quad . \tag{B.6}$$

With (B.6) the classical equations of motions are

$$\dot{\theta}_1 = p_{\theta_1} - \alpha p_{\theta_2} \cos\vartheta + \alpha p_\vartheta \sin\vartheta \operatorname{ctg}\theta_2$$

$$\dot{\theta}_2 = p_{\theta_2} - \alpha p_{\theta_1} \cos\vartheta + \alpha p_\vartheta \sin\vartheta \operatorname{ctg}\theta_1$$

$$\dot{\vartheta} = p_\vartheta \left(\frac{1}{\sin^2\theta_1} + \frac{1}{\sin^2\theta_2} \right) + 2\alpha p_\vartheta \frac{\cos\theta_1 \cos\theta_2 \cos\vartheta - \sin\theta_1 \sin\theta_2}{\sin\theta_1 \sin\theta_2}$$

$$+ \alpha \sin\vartheta \left(p_{\theta_1} \operatorname{ctg}\theta_2 + p_{\theta_2} \operatorname{ctg}\theta_1 \right)$$

$$\dot{p}_{\theta_1} = p_\vartheta^2 \frac{\cos\theta_1}{\sin^3\theta_1} + \alpha p_\vartheta^2 \frac{\operatorname{ctg}\theta_2}{\sin^2\theta_1} \cos\vartheta + \alpha p_{\theta_2} p_\vartheta \frac{\sin\vartheta}{\sin^3\theta_1} + 4 \sin\theta_1$$

$$\dot{p}_{\theta_2} = p_\vartheta^2 \frac{\cos\theta_2}{\sin^3\theta_2} + \alpha p_\vartheta^2 \frac{\operatorname{ctg}\theta_1}{\sin^2\theta_2} \cos\vartheta + \alpha p_{\theta_1} p_\vartheta \frac{\sin\vartheta}{\sin^3\theta_2} + 4 \sin\theta_2$$

$$\dot{p}_\vartheta = -\alpha p_{\theta_1} p_{\theta_2} \sin\vartheta + \alpha p_\vartheta^2 \operatorname{ctg}\theta_1 \operatorname{ctg}\theta_2 \sin\vartheta$$

$$- \alpha p_\vartheta \cos\vartheta \left(p_1 \operatorname{ctg}\theta_2 + p_2 \operatorname{ctg}\theta_1 \right) \ldots \tag{B.7}$$

In order to locate the tip of the cusp it is necessary to study the classical trajectory with $\theta_1 = \theta_2$ and ϑ infinitesimal. The point (B.1) is determined by the location on this trajectory where $\vartheta = 0$. Therefore

$$\theta_1 = \theta_2 \qquad p_{\theta_1} = p_{\theta_2} \ , \tag{B.8}$$

and (B.7) reduces to

$$\dot{\theta}_1 = (1-\alpha)\, p_{\theta_1}$$

$$\dot{p}_{\theta_1} = 4 \sin\theta_1$$

$$\dot{\vartheta} = p_\vartheta \frac{2}{\sin^2\theta_1} (1 + \alpha \cos 2\theta_1) + 2\alpha \vartheta p_\vartheta \operatorname{ctg}\theta_1 \tag{B.9}$$

$$\dot{p}_\vartheta = -\alpha p_{\theta_1}^2 \vartheta - 2\alpha p_\vartheta p_{\theta_1} \operatorname{ctg}\theta_1 \ .$$

The initial conditions are $\theta_1 \to 0$, $p_{\theta_1} \to 0$, and $p_\vartheta \to 0$ as $t \to -\infty$.

The solution of the first two equations of (B.9) is

$$\theta_1 = 4 \cdot \tan^{-1}\left(\exp\left[2\sqrt{1-\alpha}\, t \right] \right) , \tag{B.10}$$

where we have dropped an additive constant to t without losing any information. At t = 0, (B.10) gives $\theta_1 = \theta_2 = \pi$, which corresponds to the "south pole" in both B_I and B_{II}. Therefore t remains negative in the range of interest.

In order to treat the last two equations of (B.9), a convenient variable is

$$\xi = \cosh\left[4 (1-\alpha)^{1/2} t \right] , \tag{B.11}$$

Then

$$4\sqrt{1-\alpha}\sqrt{\xi^2-1}\,\frac{d\vartheta}{d\xi} + p_\vartheta \frac{1}{4(\xi-1)}\left[(\xi+1)^2+\alpha(\xi^2-14\xi+17)\right]$$

$$+4\alpha(1-\alpha)^{-1/2}(\xi-3)(\xi^2-1)^{-1/2}\vartheta = 0 \qquad \text{(B.12)}$$

and

$$4\sqrt{1-\alpha}\sqrt{\xi^2-1}\,\frac{dp_\vartheta}{d\xi} - \frac{32\alpha}{1-\alpha}\,\frac{1}{\xi+1}\,\vartheta$$

$$-4\alpha(1-\alpha)^{-1/2}(\xi-3)(\xi^2-1)^{-1/2}p_\vartheta = 0\,. \qquad \text{(B.13)}$$

If (B.13) is used to express ϑ in terms of p_ϑ, and the resulting expression is substituted into (B.12), p_ϑ is found to satisfy a known second-order ordinary differential equation with the solution

$$p_\vartheta = \zeta^{\frac{1}{2}\left[1+\left(\frac{1+\alpha}{1-\alpha}\right)^{1/2}\right]} F(a,b;c;\zeta), \qquad \text{(B.14)}$$

where F is the hypergeometric function,

$$a,b = \frac{1}{4}\cdot\left[1+2\left(\frac{1+\alpha}{1-\alpha}\right)^{1/2} \pm \left(\frac{1+15\alpha}{1-\alpha}\right)^{1/2}\right] \qquad \text{(B.15)}$$

$$c = 1+\left(\frac{1+\alpha}{1-\alpha}\right)^{1/2}, \qquad \text{(B.16)}$$

and $$\zeta = \frac{2}{\xi+1} = \frac{1}{2}(1-\cos\theta_1). \qquad \text{(B.17)}$$

The tip of the cusp on the caustic is determined by setting $\vartheta = 0$. Thus it is given by the value of $\theta_1 > 0$ where

$$\left\{\zeta\frac{d}{d\zeta} + \frac{1}{2}\left[1+\left(\frac{1+\alpha}{1-\alpha}\right)^{1/2}\right] + \frac{\alpha}{1-\alpha}\,\frac{1-2\zeta}{1-\zeta}\right\} F(a,b;c;\zeta) = 0. \qquad \text{(B.18)}$$

Alternative forms of (B.18) can be obtained by applying the quadratic transform of hypergeometric functions.

There are three values of α for which (B.18) can be solved exactly. They are:

(i) If $\alpha = 0$, then $z = 1$ and $\theta_1 = \theta_2 = \pi$;

(ii) If $\alpha = \frac{3}{5}$, then $z = \frac{2}{3}$; and

(iii) As $\alpha \to 1-$, $z \to \frac{1}{2}$ and $\theta_1 = \theta_2 \to \frac{\pi}{2}+$.

Numerical calculations have been carried out for the following three cases:

(iv) If $\alpha = \frac{1}{8}$, then $z \sim 0.951707$ and $\theta_1 = \theta_2 \sim 2.698464$;

(v) If $\alpha = \frac{1}{4}$, then $z \sim 0.864858405$ and $\theta_1 = \theta_2 \sim 2.388704014$ [This is the results (B.1)]; and

(vi) If $\alpha = \frac{1}{2}$, then $z \sim 0.714005919$ and $\theta_1 = \theta_2 \sim 2.013088107$.

Note that $\theta_1 = \theta_2$ decreases as α increases.

References

1) K.G. Wilson, Phys. Rev. D10 (1974), 2445

2) For a recent review see, for example, P. Hasenfratz' lecture in the XXIII International Conference on High Energy Physics, Berkeley 1986, to appear in the proceedings.

3) J.B. Kogut, D.K. Sinclair and L. Susskind, Nucl. Phys. B114 (1976), 199

4) G. Münster, Nucl. Phys. B190 [FS3] (1981), 439
K. Decker, Nucl. Phys. B240 [FS12] (1984), 543 and references therein.

5) M. Creutz, Phys. Rev. D21 (1980), 2308

6) K. Symanzik, Commun. Math. Phys. 18 (1970), 227; 23 (1971), 49
C. Callan, Phys. Rev. D2 (1970), 1541

7) M. Göpfert and G. Mack, Commun. Math. Phys. 82 (1982), 545

8) J. Kogut and L. Susskind, Phys. Rev. D11 (1975), 395

9) S.D. Drell, H.R. Quinn, B. Svetitsky and M. Weinstein, Phys. Rev. D19 (1979), 619
S. Ben-Menahem, Phys. Rev. D20 (1979), 1923

10) U. Heller, Phys. Rev. D23 (1981), 2357
D. Horn and M. Weinstein, Phys. Rev. D25 (1982), 3331
P. Suranyi, Nucl. Phys. B210 [FS6] (1982), 519; Phys. Letters 122B (1983), 279; Nucl. Phys. B225 (1983), 77
W. Langguth, Z. Phys. C23 (1984), 289

11) A. Patkoś and F. Deák, Z. Phys. C9 (1981), 359
A. Patkoś, Phys. Letters 110B (1982), 391
N.D. Hari Dass, P.G. Lauwers and A. Patkoś, Phys. Letters 124B (1983), 387
P. Suranyi, Nucl. Phys. B210 [FS6] (1982), 519
H. Arisue, M. Kato and T. Fujiwara, Progr. Theor. Phys. 70 (1983), 229
D. Horn and M. Karliner, Nucl. Phys. B235 [FS11] (1984), 135
J.B. Bronzan, Phys. Rev. D31 (1985), 2020; Phys. Rev. D32 (1985), 2748

12) M. Hellmund, J. Phys. G (Nucl. Phys.) 10 (1984), 859

13) D. Horn and M. Weinstein, Phys. Rev. D30 (1984), 1256
D. Horn, M. Karliner and M. Weinstein, Phys. Rev. D31 (1985), 2589
C.P. van den Doel and D. Horn, Phys. Rev. D33 (1985), 3011

14) A. Duncan and R. Roskies, Phys. Rev. D31 (1985), 364

15) M. Lüscher, Phys. Lett. 118B (1982), 391; Nucl. Phys. B219 (1983), 233
M. Lüscher and G. Münster, Nucl. Phys. B232 (1984), 445

16) V.F. Müller and W. Rühl, Nucl. Phys. B230 [FS10] (1984), 49
S. Meyer, V.F. Müller, T. Raddatz and W. Rühl, Nucl. Phys. B240 [FS 12] (1984), 400

17) P. van Baal, Nucl. Phys. B264 (1986), 548
J. Koller and P. van Baal, Nucl. Phys. B273 (1986), 387

18) C.G. Callan, R. Dashen and D.J. Gross, Phys. Rev. D17 (1978), 2717; D19 (1979), 1826

19) For a modern description of focal points and caustics see Ref. 20; other aspects of the semiclassical approximation are known from geometrical optics. For Young's phenomenon see, for example, A. Sommerfeld's book on optics: A. Sommerfeld, "Vorlesungen über Theoretische Physik", Bd. IV, Verlag Harri Deutsch 1978

20) V.I. Arnold, "Mathematical Methods of Classical Mechanics", Appendix 12; Springer Verlag 1978

21) For an introduction into phenomena of nonlinear mechanics see: A.J. Lichtenberg and M.A. Lieberman "Regular and Stochastic Motion", Applied Mathematical Sciences 38, Springer Verlag 1983 and References therein

22) See Ref. 20) and references therein. In particular: V.I. Arnold, Funct. Analiz i ego Priloshen. 6, No. 4, p. 3-25 (1972) [engl. trans.: Functional Analysis and its Applications 6:4 (1972), 254-272]
Also: V.I. Arnold, S.M. Gusein-Zade and A.N. Varchenko "Singularities of Differentiable Maps", Vol. I, Birkhäuser Monographs in Mathematics 1985

23) A. Messiah "Quantum Mechanics I and II", North Holland Publishing Company 1962

24) R. Feynman and A.R. Hibbs "Quantum Mechanics and Path Integrals", McGraw-Hill Book Company 1965

25) A. Gonzales-Arroyo, J. Jurkiewicz and C.P. Korthaus-Altes in Proc. of the Freiburg NATO Summer Institute, Plenum Press 1981

26) See for example: C.W. Misner, K.S. Thorne and J.A. Wheeler "Gravitation", W.H. Freeman and Company, San Francisco 1973

27) D. Robson and D.M. Webber, Z. Phys. C7 (1980), 53; Z. Phys. C15 (1982), 199 and references therein.

28) J.B. Bronzan, Phys. Rev. D31 (1985), 2020

29) H. Bateman "Higher Transcendental Function", Vol. II, McGraw-Hill 1953

Figure Captions

Fig. 1: Mapping of the N-dimensional Lagrangian manifold in the 2N-dimensional phase space to the N-dimensional configuration space in the simplest case N=1. (a) For each q, there is one value of $p = \frac{\partial S}{\partial q}$. (b) For each q, there are either two or no value of p depending on whether q is to the right or left of the dotted line.

Fig. 2: Single plaquette with free boundary condition.

Fig. 3: Two plaquettes with free boundary condition.

Fig. 4: The three gauge invariant degrees of freedom for the SU(2) two-plaquette problem with free boundary condition. The lines with arrows indicate the contraction of boundary planes to lines (see text).

Fig. 5: Caustics in the plane $\theta_1 = \theta_2$. Two of the interesting features are the tip of the cusp at $\vartheta = 0$ and the "bottle neck" F.

Fig. 6: Schematic drawing of the behavior of classical trajectories in the vicinity of the cusp.

Fig. 7: Caustics in the plane $\vartheta = 0$.

Fig. 8: Schematic drawings of the caustics near the "bottle neck" F.

Fig. 9: The cusp singularity in normal form. It is classified as A_3 by Arnold [20].

Fig. 10: The "bottle-neck" singularity in normal form. It is classified as D_4^+ by Arnold [20].

Fig. 11: Schematic drawing of a classical trajectory that passes near both the tip of the cusp and the "bottle neck" singularity F.

Fig. 12: The cube as the 1^3 SU(2) lattice.

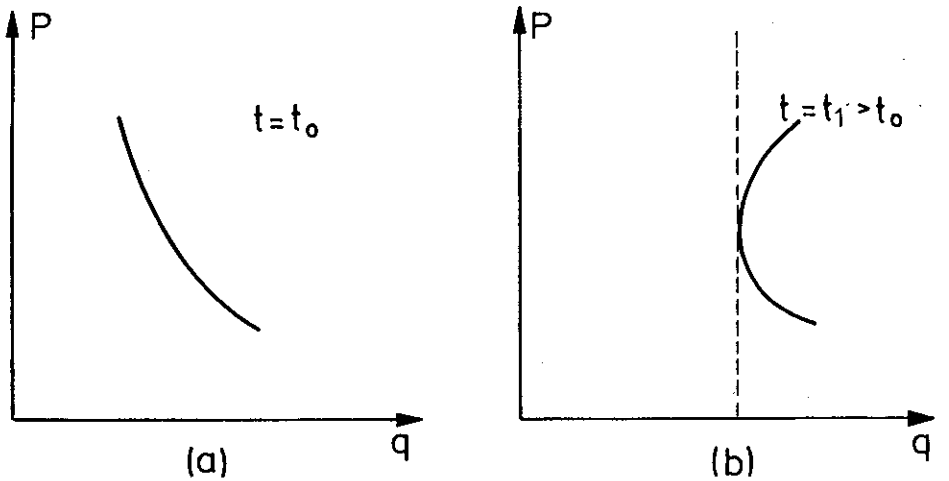

Fig.1

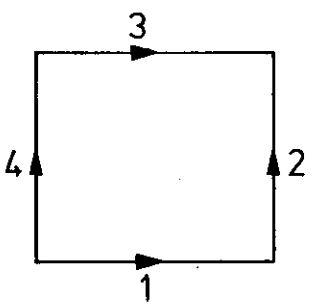

Fig.2

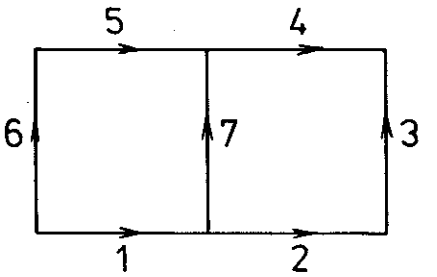

Fig.3

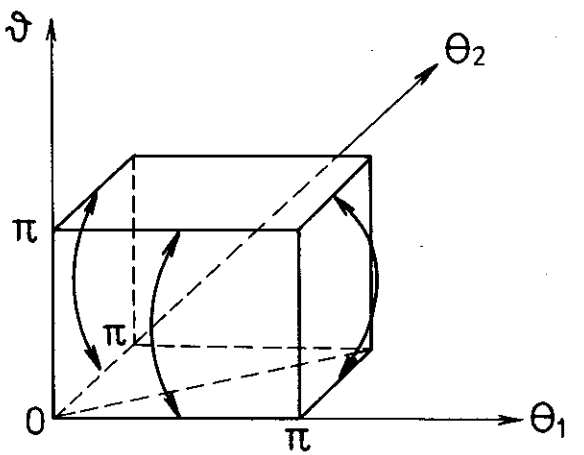

Fig.4

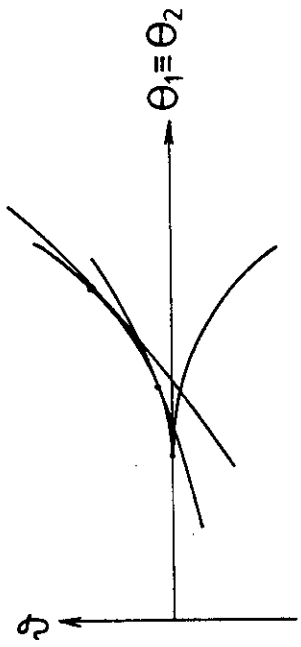

Fig.6

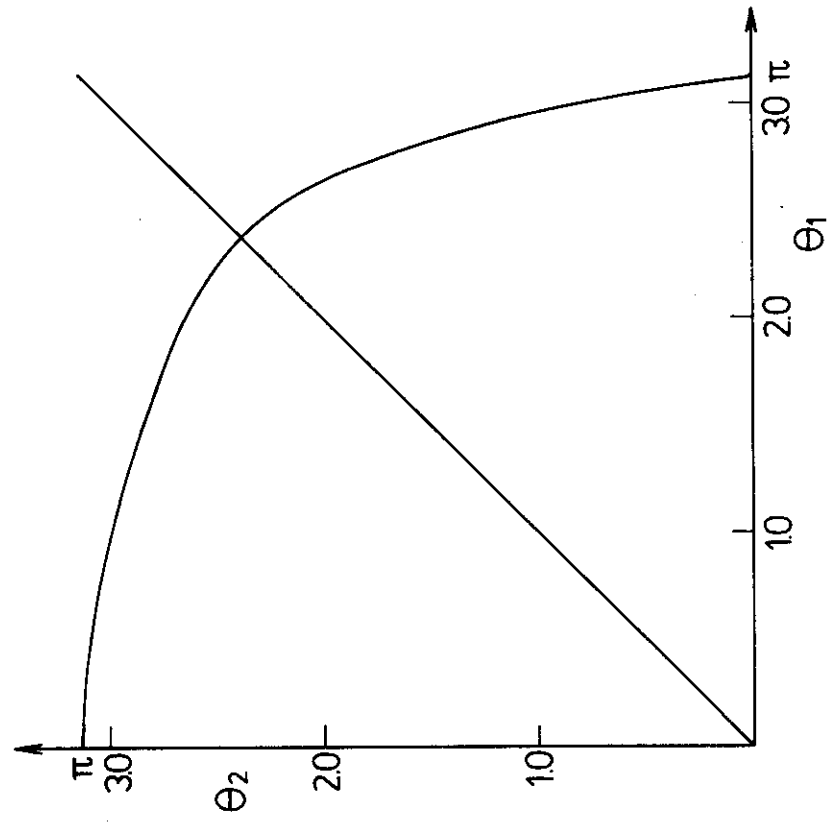

Fig.7

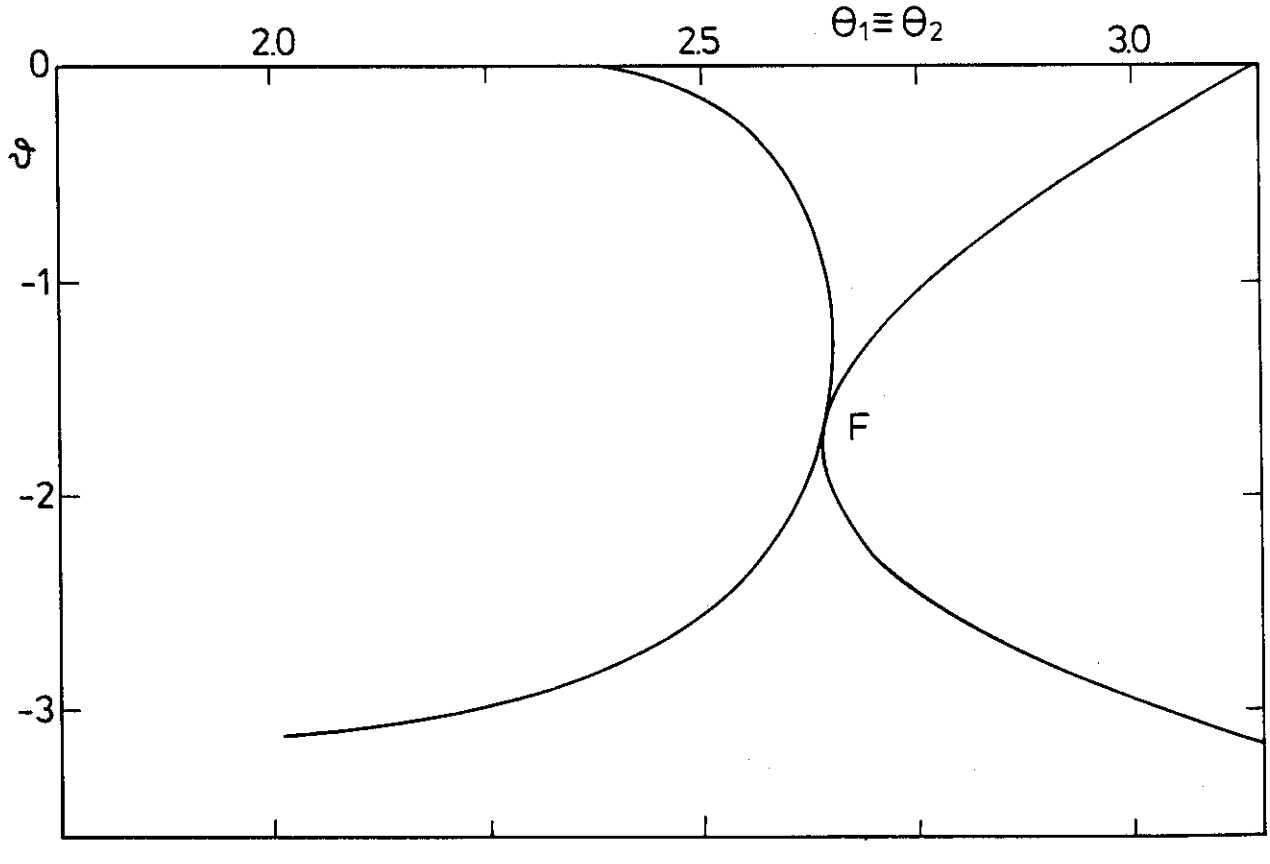

Fig.5

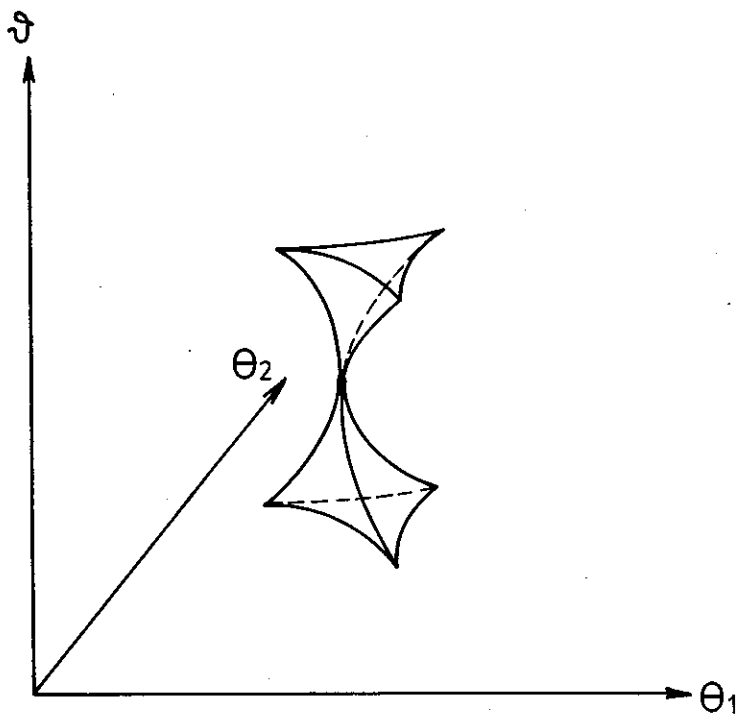

Fig. 8

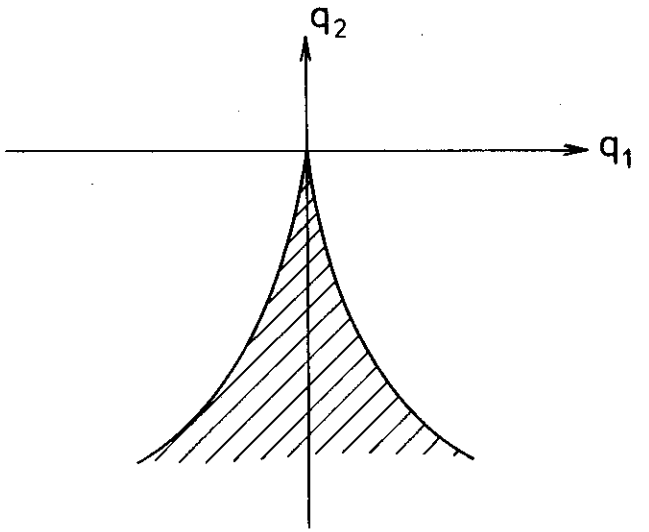

Fig. 9

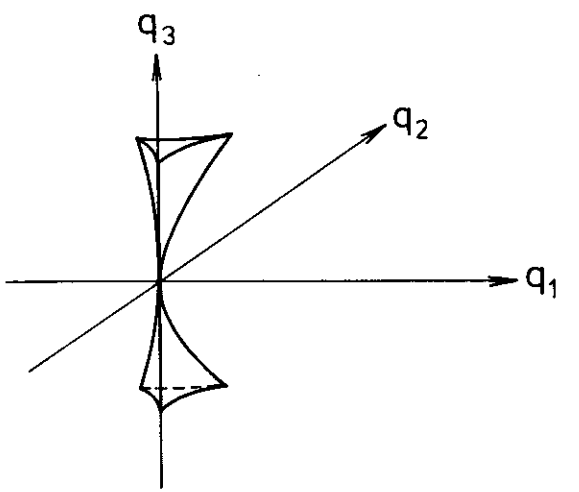

Fig. 10

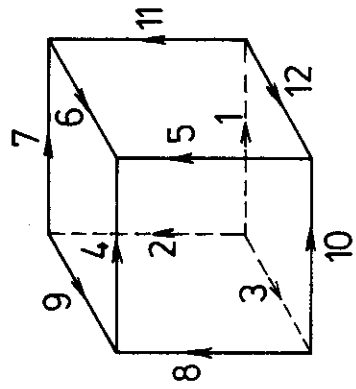
11
12
7
6
5
1
4
2
10
9
3
8

Fig.12

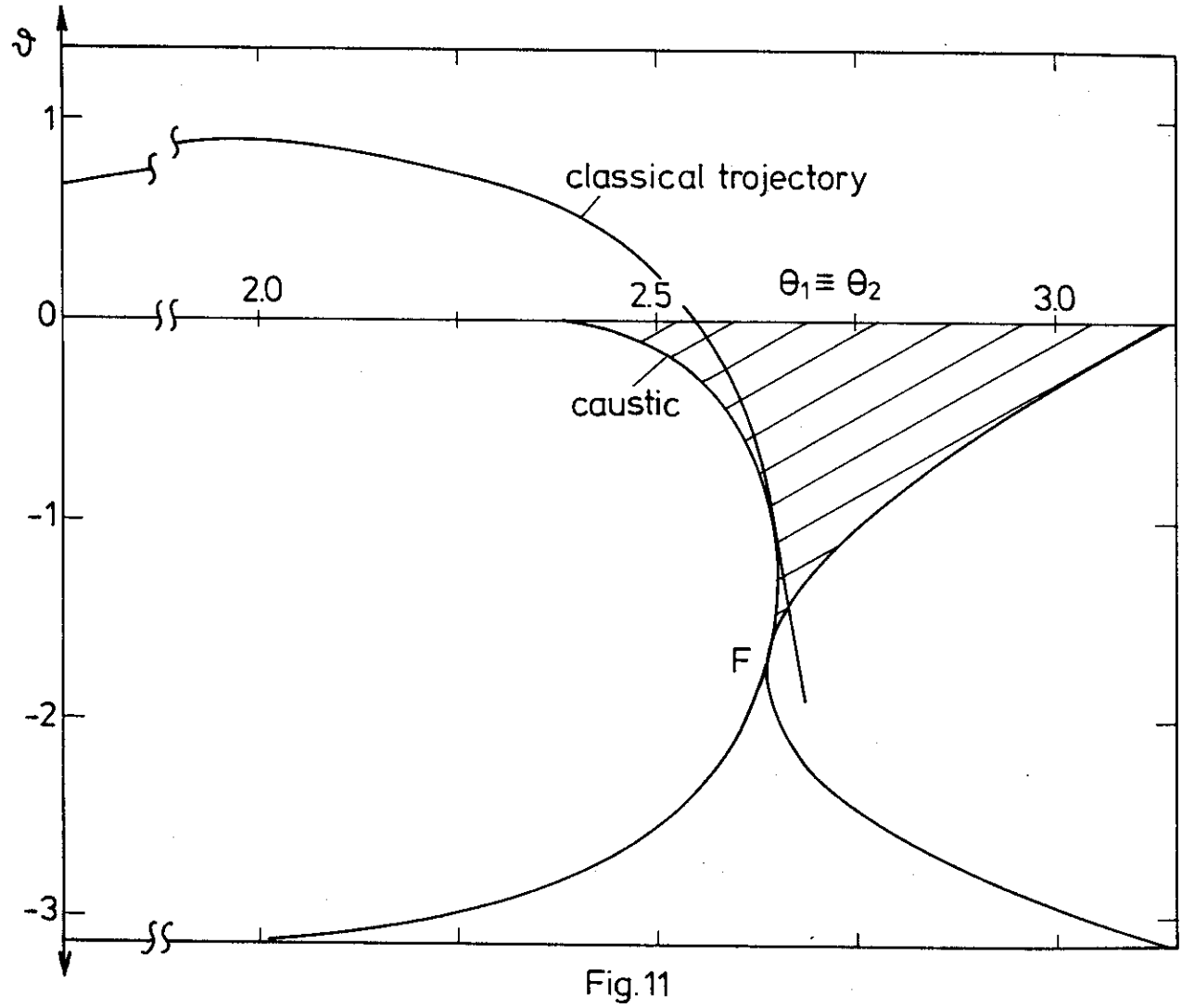
ϑ
1
0
-1
-2
-3
classical trojectory
2.0
2.5
θ1 ≡ θ2
3.0
caustic
F

Fig. 11